Chair of Drilling and Completion Engineering

Master's Thesis

Development and Test of a New Device for Geomechanical Rock Properties

Luis Arnaldo Gonzalez

September 2019

Dedicated to the memory of my parents.

AFFIDAVIT

I declare on oath that I wrote this thesis independently, did not use other than the specified sources and aids, and did not otherwise use any unauthorized aids.

I declare that I have read, understood, and complied with the guidelines of the senate of the Montanuniversität Leoben for "Good Scientific Practice".

Furthermore, I declare that the electronic and printed version of the submitted thesis are identical, both, formally and with regard to content.

Date 21.09.2019

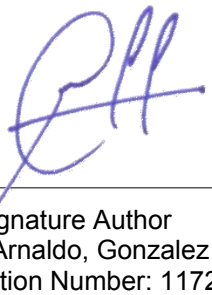

Signature Author
Luis Arnaldo, Gonzalez
Matriculation Number: 11727230

Abstract

The strength of the rock has a crucial importance in drilling engineering as it can be used to predict the ROP, drill bit optimization and to avoid wellbore stability related issues. Unconfined Compressive Strength (UCS) is one of the most generally accepted parameters used to quantify the rock strength. Determining the UCS in a laboratory requires availability of rock samples, special techniques and treatment of the samples. Therefore, it represents a high cost and cannot be done on each well that is drilled. There are other ways to determine UCS, but they all have limitations.

In this work, a novel device along with a methodology to determine UCS from rock cuttings is presented: the Rock Crusher. A series of initial tests were done using cement samples with different strengths taking the main current of the device as an indicator of the strength. These tests showed a good correlation between the mean current and the UCS of the tested material.

The concept of Specific Energy applied to rock cuttings was used, and the specific energy necessary to crush the rock was found to be a better indicator of the strength of the rock.

Finally, a series of tests on rock samples with different strength were done showing a weaker correlation between the strength and the specific energy, compared to the one of the cement samples. However, after a careful analysis of the information generated it was observed that the parameter that better describes the crushing process of cuttings is the Cohesion of the rock.

Zusammenfassung

Die Festigkeit des Gesteins ist für die Bohrtechnik von entscheidender Bedeutung, da sie zur Vorhersage der ROP, zur Optimierung des Bohrmeißels und zur Vermeidung von Problemen im Zusammenhang mit der Bohrlochstabilität angewendet werden kann.

Die einaxiale Druckfestigkeit (UCS - Unconfined Compressive Strength) ist einer der allgemein anerkannten Parameter zur Quantifizierung der Gesteinsfestigkeit.

Die Bestimmung des UCS in einem Labor erfordert die Verfügbarkeit von Gesteinsproben sowie spezielle Techniken als auch Behandlung der Proben. Dies ist mit hohen Kosten verbunden und kann daher nicht für jedes abgeteufte Bohrloch durchgeführt werden. Es gibt andere Möglichkeiten UCS zu bestimmen, die jedoch Einschränkungen mit sich bringen.

In dieser Arbeit wird ein neuartiges Gerät zusammen mit einer Methode zur Bestimmung des UCS aus Bohrgut (cuttings) vorgestellt: „The Rock Crusher“. Eine Reihe von ersten Tests wurde unter Verwendung von Zementproben mit unterschiedlichen Festigkeiten durchgeführt, wobei der Mittelstrom der Vorrichtung als Indikator für die Festigkeit herangezogen wurde. Diese Tests zeigten eine gute Korrelation zwischen dem Mittelstrom und dem UCS des getesteten Materials.

Verwendet wurde das auf Bohrgut angewendete Konzept der spezifischen Energie. Dabei stellte sich heraus, dass die zum Zerkleinern des Gesteins erforderliche spezifische Energie, ein besserer Indikator für die Festigkeit des Gesteins ist.

Schließlich wurde eine Reihe von Tests an Gesteinsproben mit unterschiedlicher Festigkeit durchgeführt, die eine schwächere Korrelation zwischen der Festigkeit und der spezifischen Energie im Vergleich zu der Zementprobe zeigten.

Nach einer sorgfältigen Analyse der generierten und erarbeiteten Informationen wurde jedoch festgestellt, dass ein bestimmter Parameter den Zerkleinerungsprozess des Bohrkleins genauer beschreibt, nämlich die Kohäsion.

Acknowledgements

Firstly, I would like to thank Univ.-Prof. Dipl.-Ing. Dr. mont. Gerhard Thonhauser for his continuous support during this this thesis project.

In addition, I would like to express my gratitude to Dr. Kristian Kohller and Prof. Dr. Jürgen Schön for their invaluable guidance, support and motivation.

Further, I would like to thank the Companies TDE Group and OMV for sponsoring the project and their teams who helped me in this project.

Contents

Chapter 1 Introduction

Among the mechanical properties of the rock, Unconfined Compressive Strength is a parameter used in drilling engineering to determine the rock strength, which can be used to avoid instability problems, stuck pipe, tight hole, wellbore collapse, pack off and sand production. It also controls the Rate of Penetration. (Amani and Shahbazi, 2013)

Several methods and tools have been developed to obtain the critical parameters for drilling optimization. Besides the determination of UCS in the laboratory, current methods for determining mechanical properties of the rock include log correlation, mathematical models, regression methods, etc. But they have limitations, as they can only be applied to a certain geographical area and they need to be constantly adjusted for a better correlation with core properties. By measuring these parameters in real time directly on the cuttings as they flow from the wellbore, the advantages are significant.

1.1 Objective of this Thesis

This thesis aims to develop both a method and a functional prototype of a device to characterize on-site the mechanical properties of cuttings.

For this purpose, the physics behind rock crushing mechanisms have to be understood in order to be able to build the device and to test the methodology. The device will be tested with sampling material whose mechanical properties will be previously determined in a laboratory. Once the data has been collected, a statistic analysis for data consistency will be done, and then final conclusions will be drawn to define the next steps in order to transfer the technology to the industry.

Chapter 2 Geomechanical Properties of Rocks

This chapter briefly describes the fundamental geomechanics properties of rocks.

2.1 Stress and Strain

As a result of a load, stress is present, and it is equal to the force acting divided by the area. It can be normal (perpendicular to the area) or shear stress acting parallel to the area). A rock that is under stress responds with a deformation, that is called strain. This deformation can be in shape, length or volume (Schön, 2015; Tiab and Donaldson, 2012; Zoback, 2007)

In the simplest case, the vertical stress σ_v in the rock is due to the overburden load, and can be calculated as follows:

$$\sigma_v = g * \int_0^z \rho(z) * dz \tag{1}$$

Where

g = earth gravity acceleration

z = depth

$\rho(z)$ = density at depth (z)

The horizontal stress σ_h is expressed as:

$$\sigma_h = \frac{\upsilon}{1-\upsilon} * \sigma_v \tag{2}$$

Where

υ = Poisson's ratio

σ_v = vertical stress

2.2 Laboratory Techniques

The mechanical properties of rocks are determined in laboratories analysing the response in deformation when known stresses are applied to rock specimens under standard conditions.

Mainly two types of parameters are determined:

1) Static Elastic Moduli
2) Strength Properties

A typical laboratory set up is the triaxial cell, shown in Figure 1. It consists of a load frame where the rock specimen is placed between the loading cylinders, which apply the vertical

stress (σ_v). Around the rock there is a sleeve which contains the axial pressure to generate the horizontal stress. Different types of sensors are used to measure the strain in the rock.

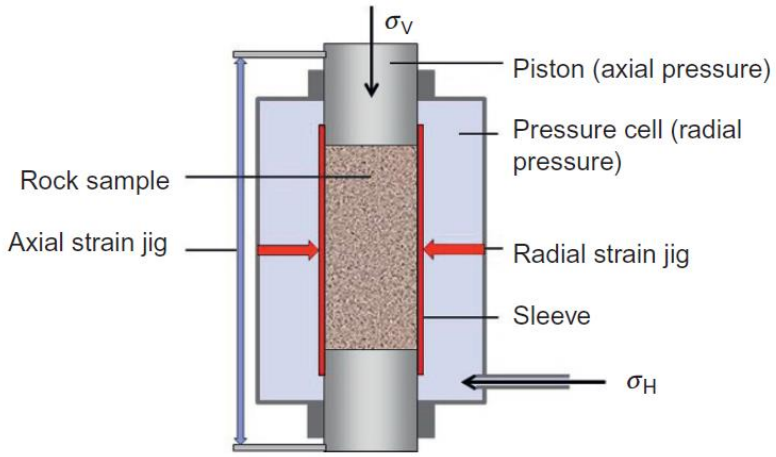

Figure 1. triaxial cell used in laboratories to test rock specimens.
Reference: Schön, 2015

A typical test curve is shown in Figure 2. When the axial force is applied, certain well-defined stages can be identified:

1) At the beginning of the test, all the cracks present in the rocks are (partially) closed as the stress increases
2) A linear elastic zone is present, since all the cracks are closed and the rock starts to be compressed. This is the preferred zone used to determine the elastic module (E).
3) As the stress is increased, new cracks are formed in the rock and it fails when the maximum compressive strength is reached.
4) A sliding process takes place once the rock has failed.

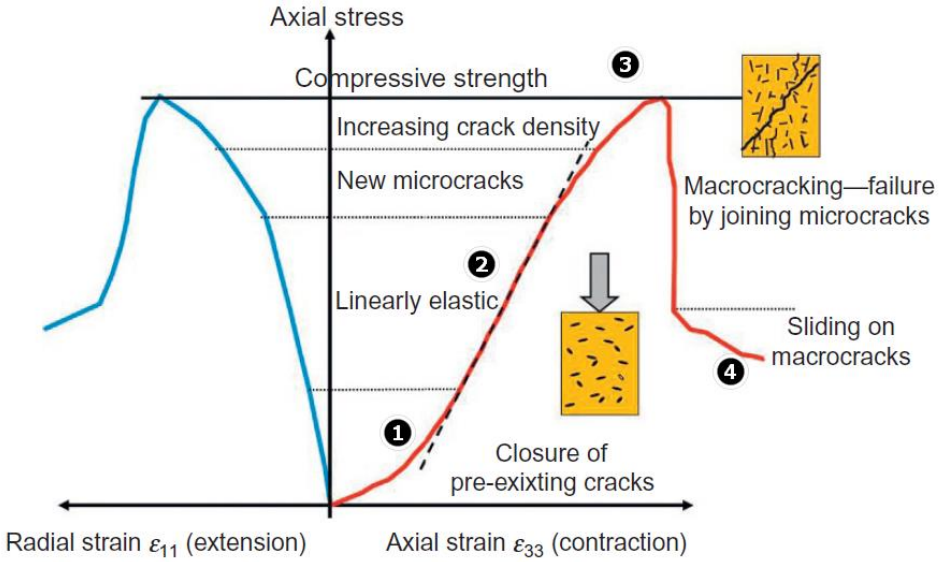

Figure 2. Strain-stress curve during a compression test of a rock specimen.
Reference: Schön, 2015

2.3 Deformation Properties

These properties are derived from a static compression test.

Young's Modulus **E** is the ratio of the axial stress and the axial strain:

$$E = \frac{\sigma}{\varepsilon} \tag{3}$$

As mentioned before, it is derived from the linear part of the strain stress curve.

Poisson's ratio $\boldsymbol{\upsilon}$ is the ratio of radial strain and axial strain:

$$\upsilon = \frac{\Delta r/_r}{\Delta l/_l} \tag{4}$$

2.4 Rock Strength Properties

The strength refers to the amount of stress applied to the rock at failure.

The most used failure criteria was proposed by Coulomb in 1773 and states that the failure is caused by a shear stress τ acting on a plane that is a function of the cohesion c of the material and the normal stress σ_n acting on the plane multiplied by the coefficient of internal friction μ of the rock (or the angle of internal friction ϕ), according to the expression:

$$\tau = c + \tan\phi * \sigma_n \tag{5}$$

Mohr suggested a graphical way to illustrate stresses in 2D, which is perfectly applicable to a triaxial test where $\sigma_{11} = \sigma_{22}$. This representation is called the Mohr's Diagram, and is shown in Figure 3:

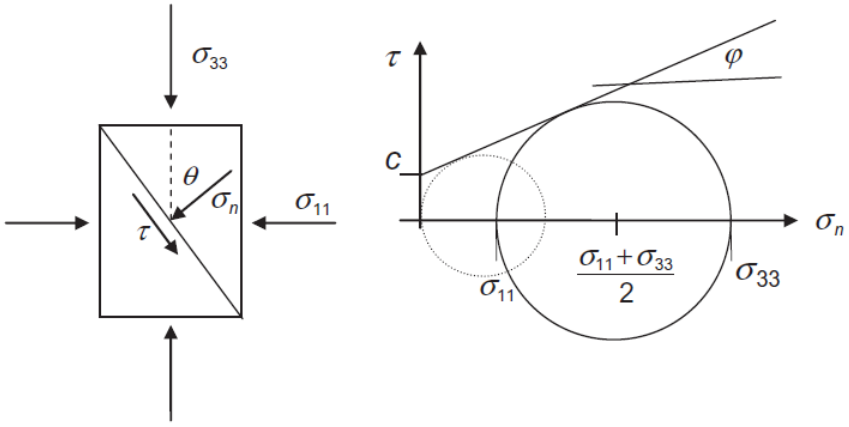

Figure 3. a) stresses acting in a rock specimen. b) Mohr circle.
Reference: Schön, 2015

This diagram shows the relationship between the shear stress and normal stress at failure. By conducting a series of tests with different values of sigma 1 and sigma 3, one can obtain the envelope of failure, that can be considered a straight line (Figure 4). The interception of the straight line with the vertical axis is called cohesion of the rock (C) and the slope is the coefficient of internal friction.

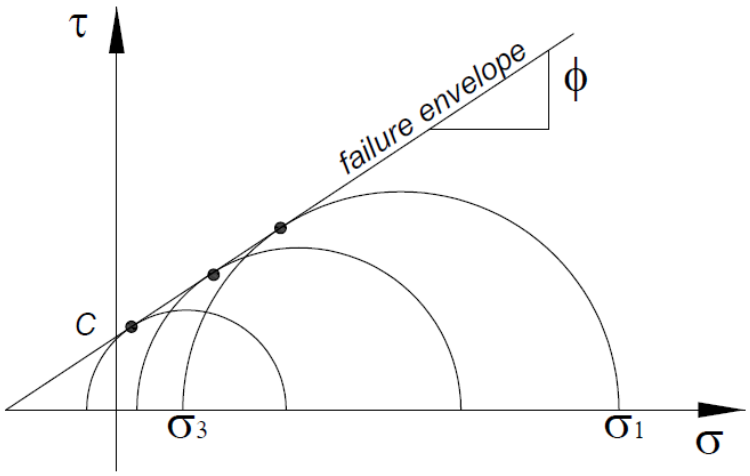

Figure 4. Mohr circle of a rock tested with different stresses.
Reference: Richard E. Goodman (1989, modified)

Coulomb's Failure Criterion -shows the relationship between stress and rock properties:

$$\sigma_{33} = \sigma_{11} * tan^2(45 + {}^{\varphi}/_{2}) + 2 * c * tan(45 + {}^{\varphi}/_{2}) \quad (6)$$

When $\sigma_{11} = 0$, the UCS results:

$$\sigma_{33} = \sigma_c = 2 * c * \tan(45 + {}^{\varphi}/_{2}) \quad (7)$$

This equation is very useful to determine the UCS from triaxial tests, knowing the cohesion and the angle of internal friction.

According to Schön (2015), the strength properties of rocks depend mainly on:

- The type and quality of mechanical bonds between the solid particles of the rock (grains).
- The presence of defects in the rock
- The internal rock structure (lamination, anisotropy)

2.5 Measurement of UCS in the Laboratory

The Unconfined Compressive strength is measured in a laboratory in the unconfined compression test. Here a specimen of rock is placed in the loading frame without confining pressure, unlike a triaxial test where confining pressure is applied (Figure 5). Then the load is increased until the specimen fails. The axial and diametral strain are monitored to generate a strain- stress curve.

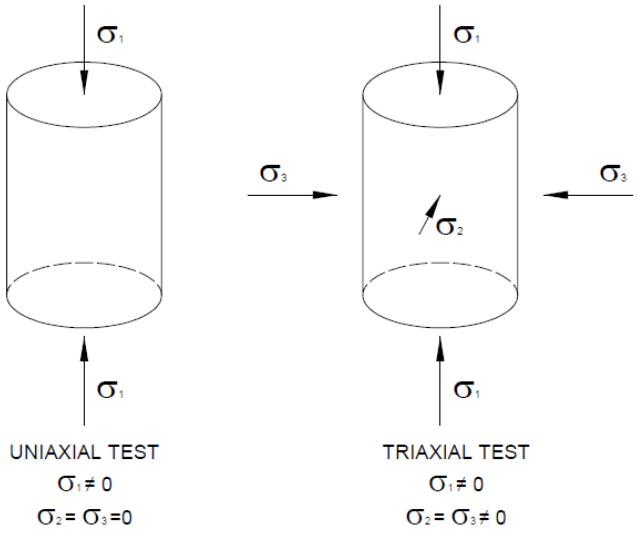

Figure 5. Uniaxial Compressive Test and Triaxial test on rock specimens. Reference: Zoback, 2007

The brittleness of a rock can be appreciated in the Strain-Stress curve (Figure 6). Once the maximum compressive stress has been reached, in a ductile material the strain continues at the same stress level, while in a brittle material the stress rapidly decreases to zero with the same strain level (Hudson and Harrison, 1997).

Most of the tested rocks have a brittle behavior, therefore it is easy to determine the maximum force applied to the specimen.

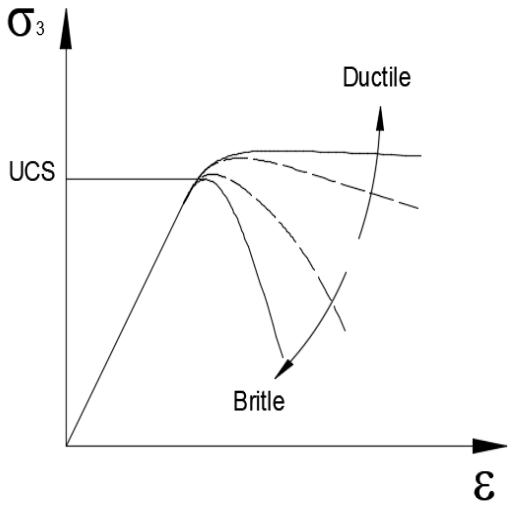

Figure 6. Strain-Stress curve of rock specimens
Reference: Hudson and Harrison, 1997

Although this is the only way to measure the UCS of the rock, this method implies high costs and it is time consuming due to the process involved in core extraction, transportation, handling and storage. It is also important to mention that usually cores are available for the reservoir section, as it could be extremely costly to have cores for the entire wellbore. This test is destructive, and so it is always difficult to have cores available to be tested.

Chapter 3 Literature Review

3.1 Applications of UCS

3.1.1 Mechanical Earth Model to Predict Instability Events

One of the main applications of the UCS is as an element of a mechanical earth model to predict instability events.

The Mechanical Earth Model (MEM) is a representation of the current stress status in a certain area, that is used to plan for drilling operations to recover hydrocarbons (Plumb et al., 2000).

By knowing the stresses in a certain area, it is possible to determine the failure modes and predict instability events due to stress concentration around the wellbore.

As different rock layers have different properties, it is essential to know their properties to predict their behavior during drilling operations. Each rock type deforms in a different way according to the in-situ stresses at a given depth. A mechanical earth model provides information about mechanical rock properties, stress regime, stress orientation, overburden stress, fluid pressure.

The MEM is composed of many elements, such as pore pressure data, overburden stress, rock strength (UCS), elastic moduli, stress orientation and regime, etc. All this information is combined to obtain these properties along the depth (Figure 7). These values can be obtained from different sources, such as seismic data, well logs, temperature logs, pressure measurements, measurements in laboratories, etc.

The MEM is calibrated with direct measurements in situ or in the laboratories and comparing actual events during drilling operations with the predictions from the mechanical earth model.

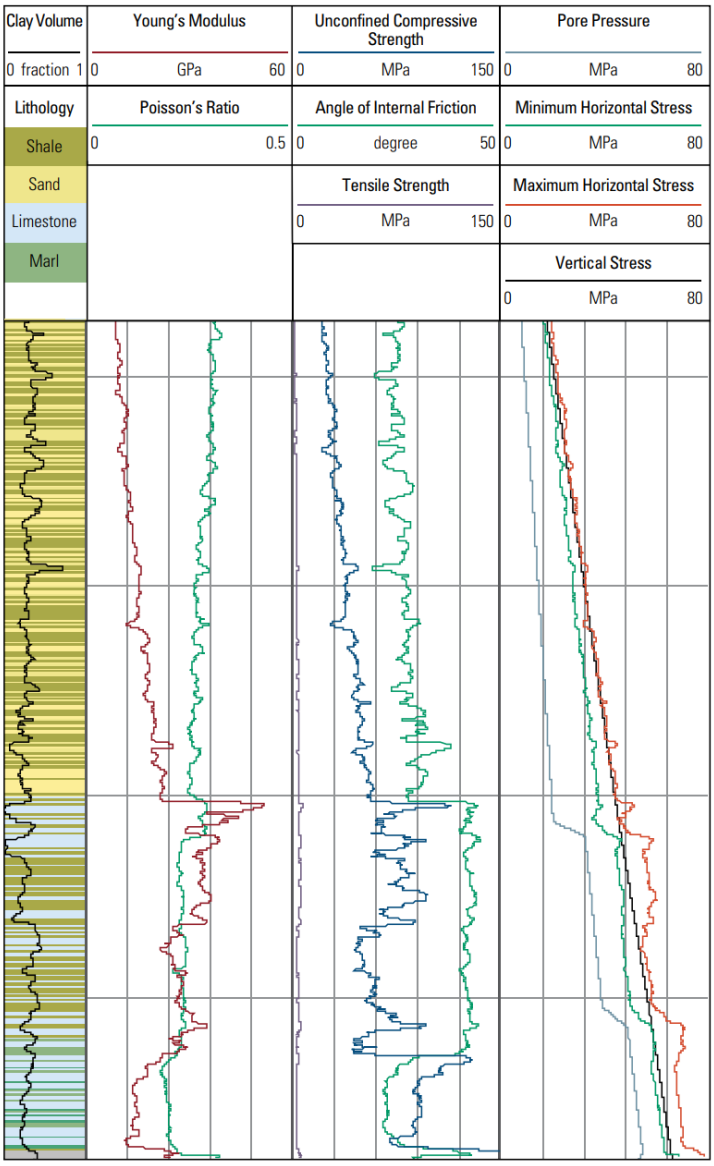

Figure 7. MEM.
Reference: Schlumberger, 2016

Some applications of the Mechanical Earth Model are (Afsari et al., 2009):

- Prediction of pore pressure and fracture gradient to design a safe mud window. Stuck pipe and drag are caused by cavings due to breakouts in the wellbore. This occurs at 90 degrees from the maximum horizontal stress when the hoop stress at the wellbore wall is bigger than the compressive strength of the rock.
- In addition to the traditional pore pressure and fracture pressure curves, it contains the upper and lower margin curve for mud weight, as a result of tensile and compressive failure of the rock.
- Although they are undesirable, breakouts are not problematic if the width is kept below a certain limit, provided that good hole cleaning practices are in place and the mud properties are adequate to clean the cavings generated.

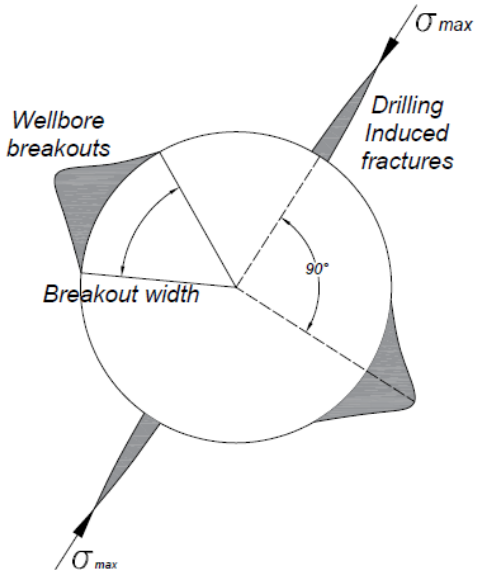

Figure 8. Breakouts and tensile induced fractures in the wellbore.
Reference: Talebi et al, 2018

Many investigations showed that an acceptable value of breakouts width is 90° (Figure 8), and it should be considered to define the lower limit of the safe mud window (Figure 9). When the width of the breakouts reaches 90°, the majority of the wellbore wall has failed , causing washouts and even the collapse of the entire wellbore, leading to the mentioned consequences (Zoback, 2007).

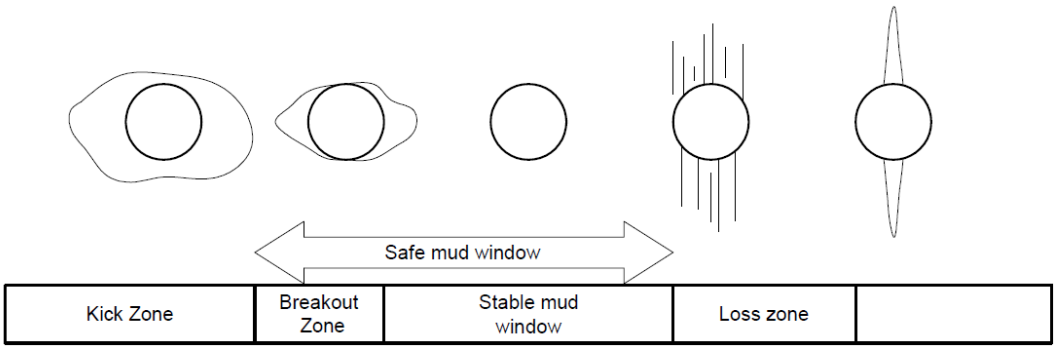

Figure 9. Safe mud window used to design mud weight for each well section.
Reference: Afsari et al., 2009

- Risk reduction of wellbore stability related incidents. These incidents can cause extra costs due to stuck pipe, fishing operations, extra wiper trips, sidetracks, etc.
- Selection of proper completion and safe pressure drawdown to avoid sand production.
- Understanding of pore pressure drop in the reservoir due to depletion, causing changes in the effective stress in the reservoir.
- Real-time decision while drilling using 3D MEM. There are many successful cases (Santarelli et al., 1997) where a Mechanical earth model was applied in real-time to

monitor and control the drilling process. A plan is made based on an integrated approach to create a MEM. During drilling, real-time data is then used to monitor the stability condition of the well, updating the MEM in real-time. This allows the operator to predict possible instability events real-time data acquired from the formations being drilled in a more accurate way and measure the effectiveness of the measures taken.

3.1.2 Drill Bit and ROP Optimization

In drill bit optimization analysis, the strength of the rock plays an important role, as the bit wear depends mainly on rock strength and silica content of the rock, among other factors. It is used to characterize the rock to be drilled to select the most appropriate cutting structure and other bit parameters, along with hydraulic parameters and gauge protection design.

Uboldi et al. (1999) showed the importance of measuring directly in the field the UCS and its benefits for improved accuracy and better model results. They performed an integrated drill bit optimization system, using UCS from measurements in the field obtained with the indentation test. The main advantages of the use of the indentation test to determine the drillability of the rock are:

- It provides a direct measurement on-site of a mechanical property of the rock.
- It provides continuous monitoring in real-time of the rock strength for an entire section of the wellbore being drilled.
- As it is a real-time measurement, it gives the possibility to adjust the prognosed strength with real values measured to adjust the model.

Although it has some limitations, this methodology has proven to be a reliable way to be used in drill bit optimization.

3.1.3 Sand Production Prediction

Sand production in the oil industry can cause several problems, such as erosion in pipelines, valves and equipment, plugging flowlines and deposition of solids in separators. Besides the high costs related to maintenance, repairs and losses in production, it represents a big safety risk in high-pressure wells and equipment because of erosion.

Sand production is a very common phenomenon that takes place in wells producing fluids from the subsurface. The whole process can be divided into three defined stages (Denney, 2003):

- Loss of integrity of the rock around the wellbore or the perforations
- Detachment of the sand particles from the rock due to drag forces caused by the fluids being produced
- Transportation of the particles by the formation fluids

At the subsurface, exists an equilibrium of stresses in the rock wall. Due to production, the depletion of the field leads to a rearrangement of in situ stresses in the rock mass. As a

consequence, the in-situ stress can exceed locally the rock strength at a certain depth, leading to the loss of mechanical integrity of the rock.

As the main parameter governing this mechanism is the rock strength, this is one of the most important properties used to create a model for sand production prediction. This information helps production and completions engineers to design the most optimum production method and the adequate pressure drawdown to minimize sand production, or to determine whether it is necessary to apply sand production measures.

3.2 Current Methods used to estimate UCS

3.2.1 UCS from Geophysical Logs

To address the problem of availability of cores, several empirical methods have been developed to estimate UCS from geophysical well logs. In some cases, this is the only way to estimate UCS due to the absence of cores for lab tests in a certain field. These methods are based on the fact that some parameters affecting the strength are the same that affect other properties such as sonic velocity, porosity and elastic properties. All these correlations must be calibrated with core measurements when available. When no cores are available for calibration, the best option is to use empirical correlations that are based on other physical properties that can be measured (Chang et al., 2006; Zoback, 2007).

(Chang et al., 2006) summarized empirical relations and compared with laboratory-determined rock properties.

Almost all the equations used to estimate UCS are based on one of the following parameters:

- P-wave velocity (V_P), or its reciprocal interval transit time ($\Delta t=V_P^{-1}$), which is directly measured in the sonic log.
- Young´s Modulus, calculated from density and velocity
- Porosity (φ), calculated from density logs assuming rock matrix and fluid density.

The reason for this is shown in Figure 10, Figure 11 and Figure 12, where we can see the different relationships between rock strength and these parameters using lab data for different rock types: sandstone, limestone and dolomite.

Although there is a significant dispersion in the data, the plots show a clear increase of the rock strength with Young´s Modulus and a decrease with porosity and V_P.

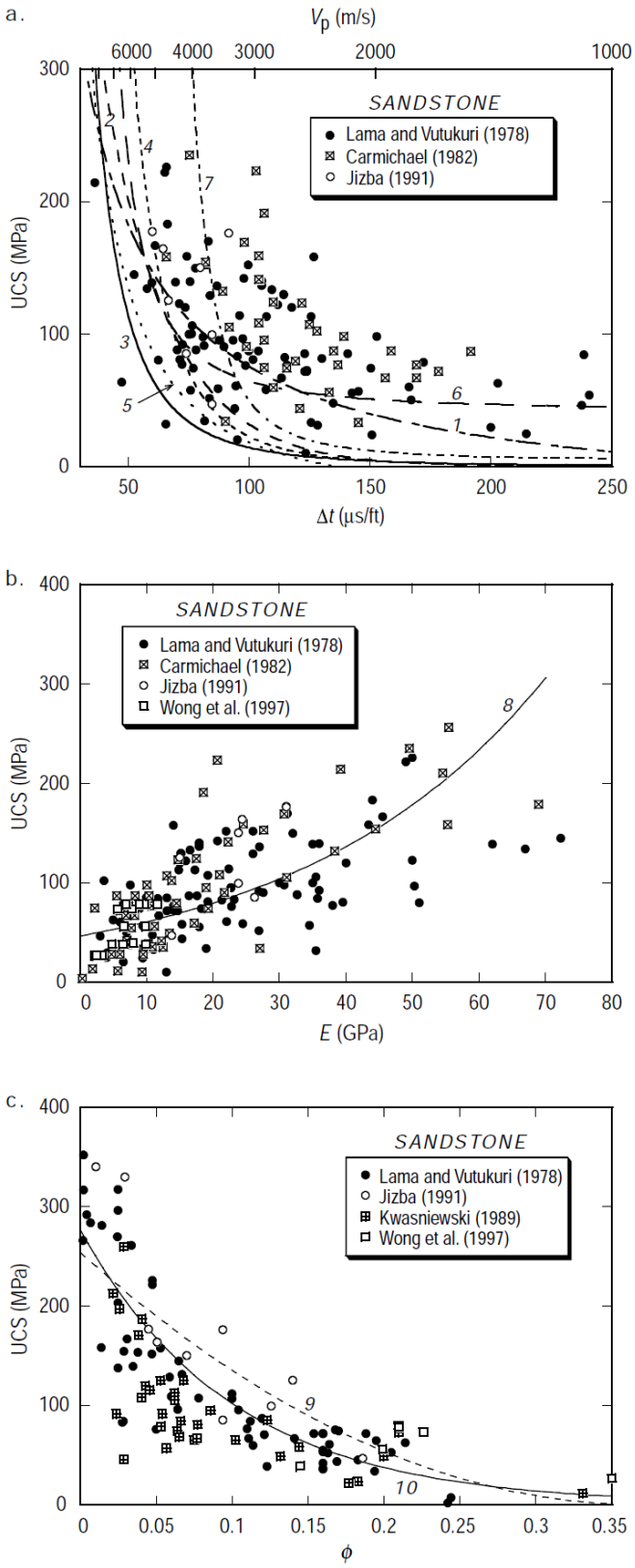

Figure 10.Comparison of different empirical equations from table 8 for different types of Sandstone.
Reference: Chang et al. , 1999

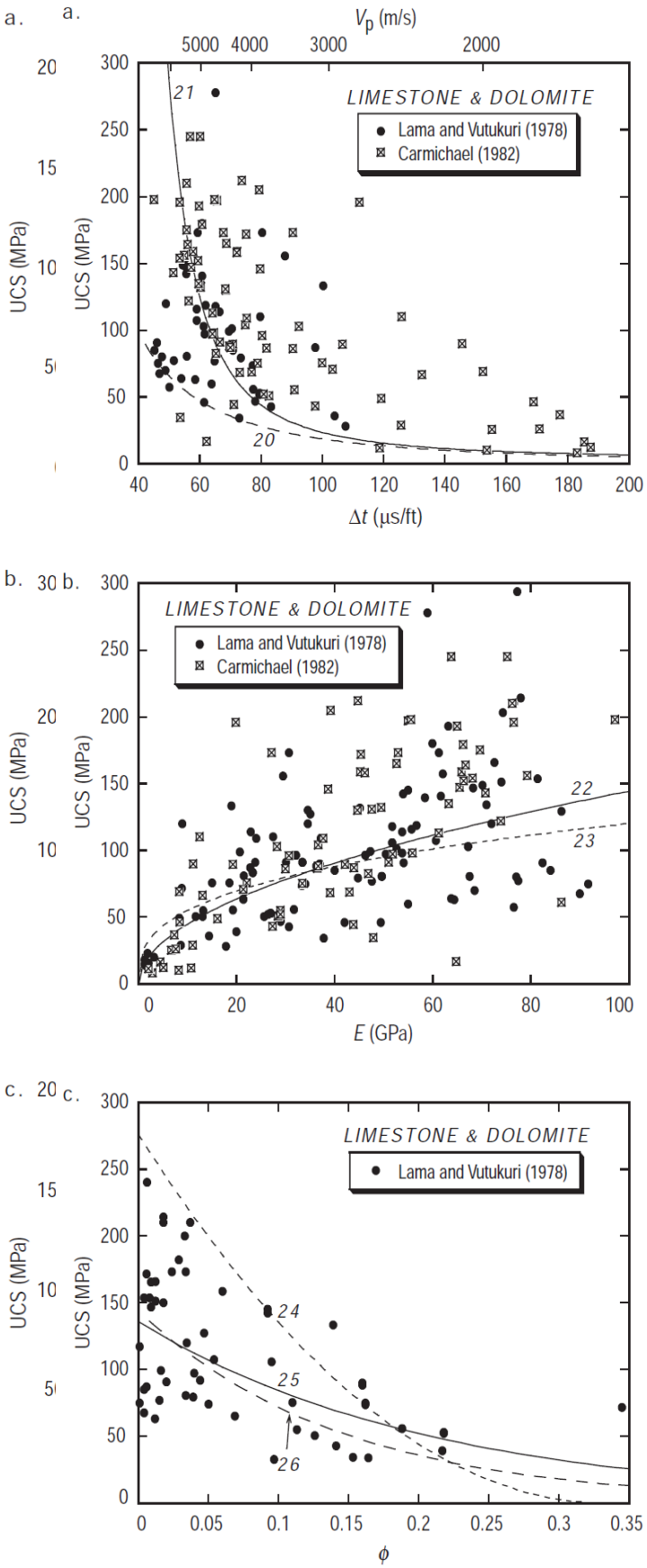

Figure 12. Comparison of different empirical equations from table 10 for different types of Limestones and Dolomites.
Reference: Chang et al., 1999

Table 8, Table 9 and Table 10 (presented in Annex A) show different empirical equations to estimate UCS in different rock types. As we can see, there are several ways to calculate UCS based on these equations. One needs to be careful when applying these relationships, because they were developed for specific areas around the world, and calibration results crucial.

In the same research work, Chang et al. (2006) determined the UCS from geophysical logs for a shale section of a vertical well in the Gulf of Mexico to show the application of these empirical equations (Figure 14 and Figure 13).

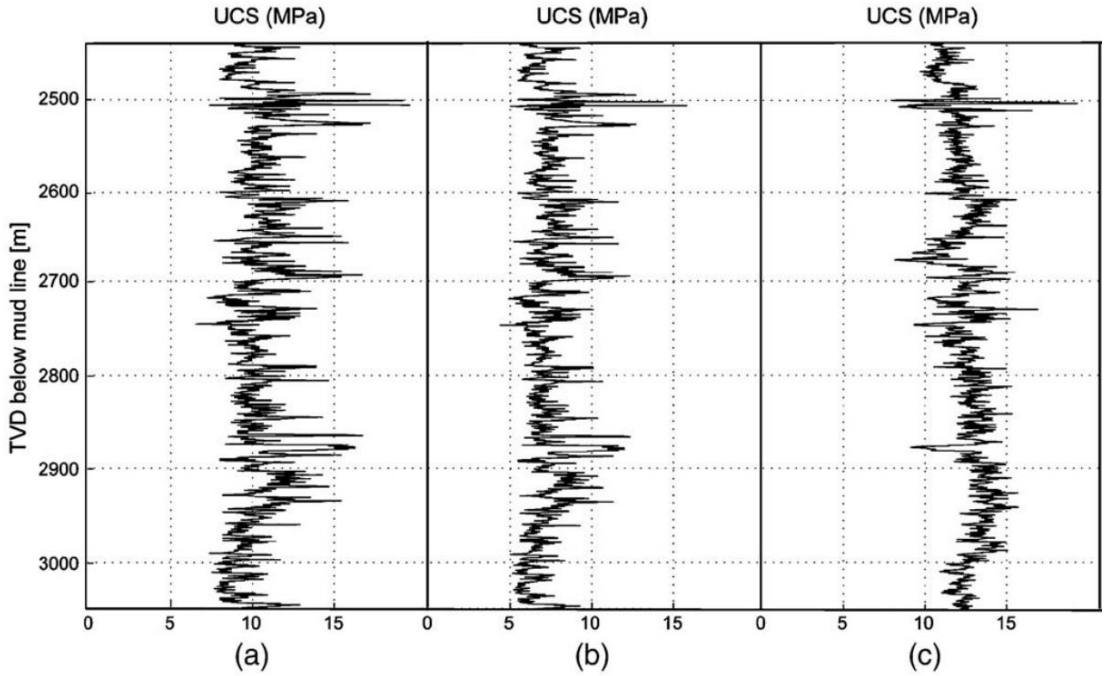

Figure 14. Different values of UCS calculated for a section of a well in the Gulf of Mexico using equations 12, 13 and 20 from Table 9 for a), b) and c) respectively. Reference: Chang et al. , 1999

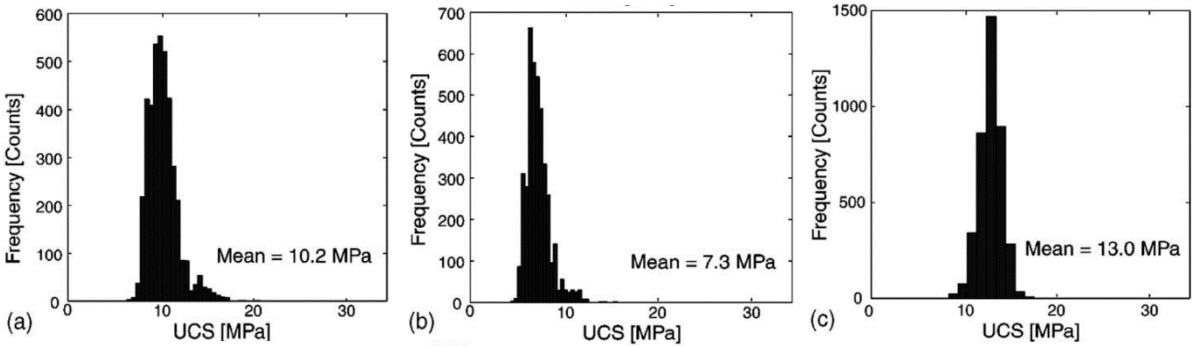

Figure 13. Frequency histograms of UCS shown in Figure 9. Reference: Chang et al., 1999

As mentioned before, there are several equations derived from geophysical logs to determine the rock strength. The best option always is to use the correlations that were developed for the region being studied, and better yet, to calibrate the obtained values with core measurements done in the laboratory.

3.2.2 Indentation Test

This test is performed on rock cuttings by embedding them in an acrylic resin in disc-shaped molds. The resin holds the cuttings in place during the test and provides the confinement necessary to avoid their tensile splitting. Then, one face of the disk is polished to leave the cuttings exposed to perform the test. During the test, a cylindrical indenter of 1 mm diameter is pushed through the cutting up to a penetration of 0.3 mm. The force and displacement of the indenter are measured continuously and plotted. The slope of this curve is called Indentation number. Usually a set of indentation test is performed to represent statistically the strength of the drilled formation.

The methodology was tested in the laboratory in different sedimentary rocks, showing a very defined relationship between the indentation number and the UCS (Santarelli et al., 1998).

Results are shown in Figure 15:

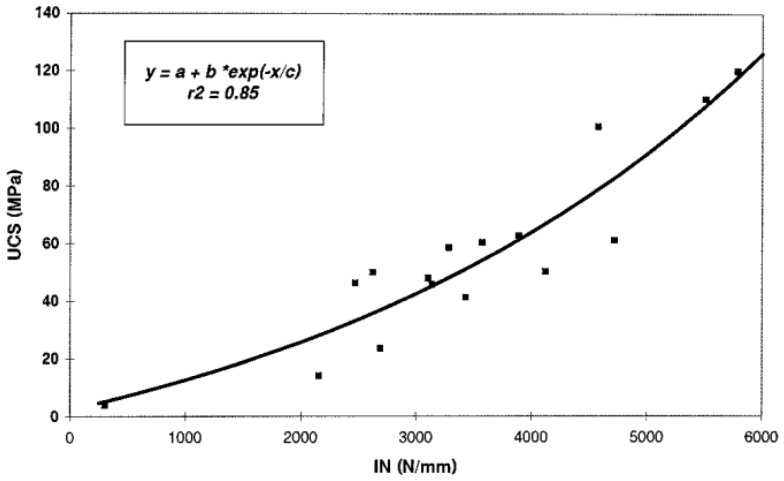

Figure 15. Correlation between indentation number and UCS.
Reference: Santarelli et Al., 1998

3.2.3 Measurement of UCS on Reconstructed Cores from Cuttings

Mazidi et al. (2012) presented a methodology to estimate the UCS of rock by using reconstructed cores from cuttings.

A total of 23 blocks of Limestone from Asmari and Sarvak formations (western Iran) were collected, as well as from Cretaceous Limestone from Northern Iran. The cuttings were generated, and the rock reconstructed from these cuttings in the form of blocks. Then, the plugs to be tested were drilled out from the blocks. The particle size used to reconstruct the rock was between 0.075 and 0.425 mm. The optimum water content was found to be between 10% and 11.6%, and the dry density of the reconstructed rock was 80% of that of the original rock. Finally, the reconstructed cores were tested according to the ASTM D2166-85 standard.

The resultant UCS values from reconstructed cores (q_u) were plotted in a cross plot vs. the UCS of the intact rock (Figure 16):

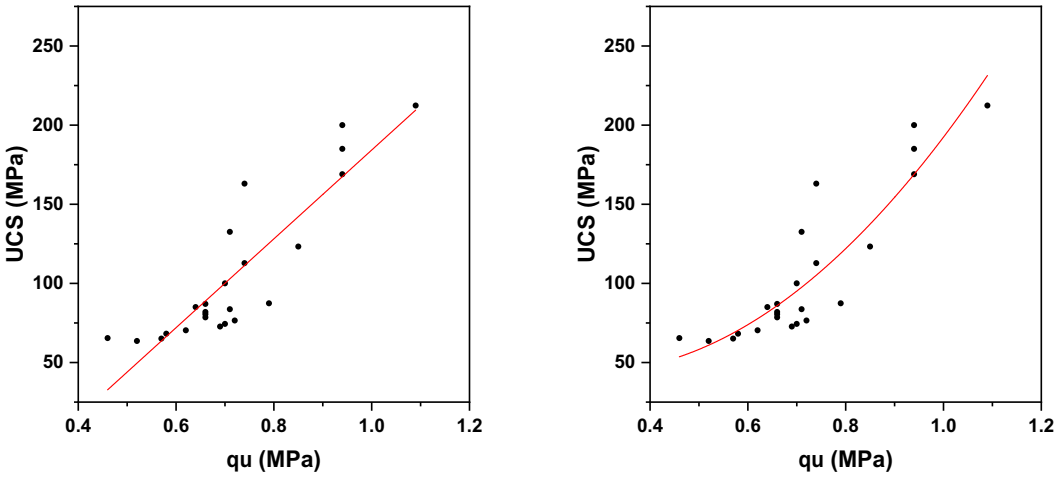

Figure 16. Cross plot showing the relationship between UCS and q_u .
Reference: Mehrabi Mazidi et al., 2012

As we can see, linear and quadratic relationships were established, with a better fit with the quadratic relationship:

Linear: $UCS = 279.8 * q_u - 95.89 \qquad R = 0.87$

Quadratic: $UCS = 280 * (q_u)^2 - 152 * q_u + 64.25 \qquad R = 0.89$

These results show that the UCS from reconstructed cores show a correlation with the one from the intact rock, and in a next step these correlations were verified with another set of reconstructed cores, as shown in Figure 17, represented with blue points.

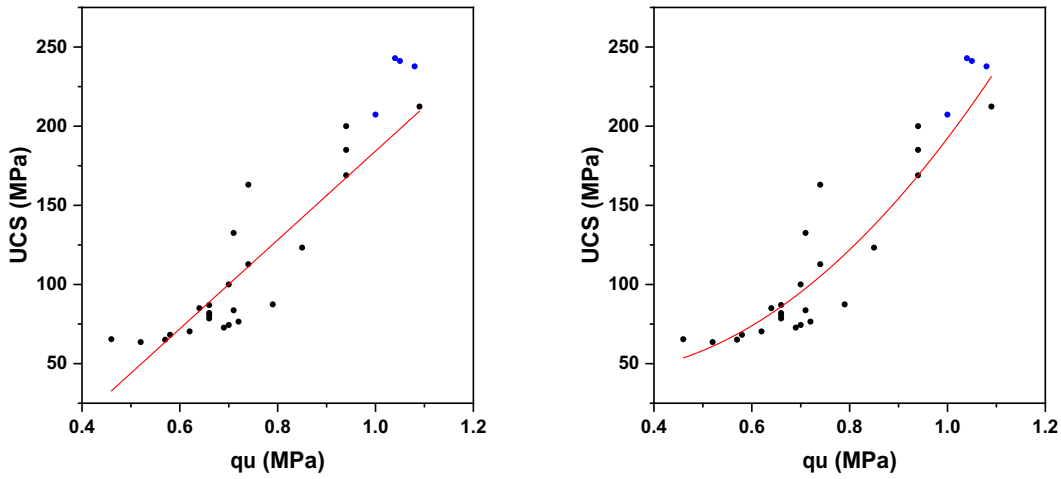

Figure 17. The blue points represent the new tests performed.
Reference: Mazidi et al., 2012

Although the method showed to be an economic estimation for UCS, there is no information about the cementing material used to form the specimens and hold in place the cuttings and its influence on the results of the Uniaxial Compressive Test.

3.2.4 Scratch Test

The scratch test consists of creating a groove on a rock specimen with a cutting tool and record the forces required to create the groove. There is experimental evidence (Richard et al., 2012) that shows the linear relationship between the specific energy applied during the test (ε) and the UCS of the rock being tested (q) (Figure 18).

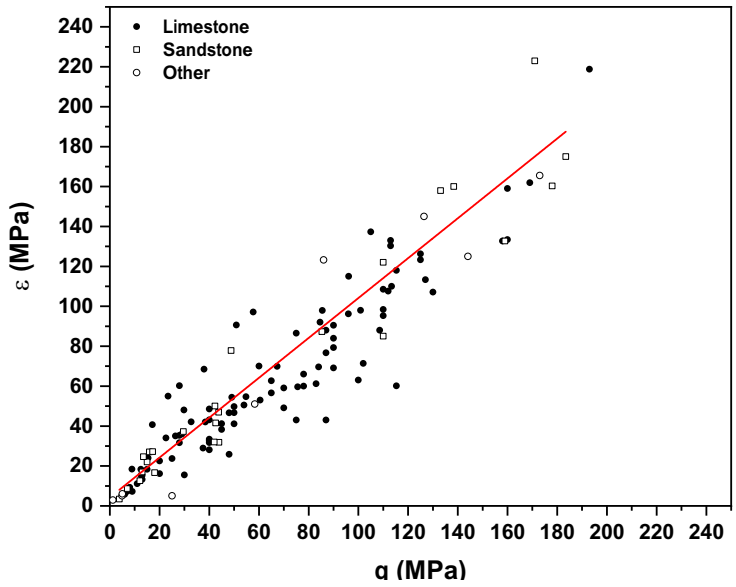

Figure 18. Correlation between the specific energy ε and the unconfined compressive Strength **q**.
Reference: Richard et al., 2012

The test is done with the rock strength device (Detournay et al., 1997), which scratches the rock in controlled kinematic conditions at a constant velocity and measures the components of the force acting on the cutter at a sampling rate of 50 Hz with a resolution of 1 N in a range of 0 to 400 N. The penetration of the cutter is also maintained constant during the test. A schematic of the device is shown in Figure 19.

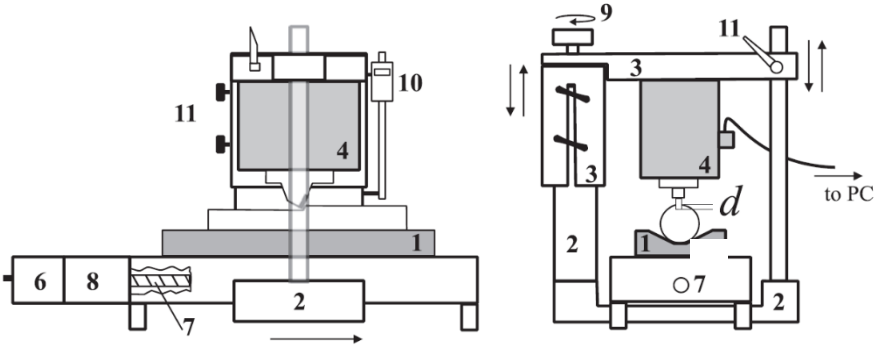

Figure 19. Schematic of the Rock strength Device

The main advantages of the test are (Richard et al., 2012):

- Repeatability- several tests performed on homogeneous rock showed little dispersion of the measured forces.
- The test can be done in the rock samples without affecting the integrity of the specimen, which then can be used for compressive tests for further studies.
- All the tests performed show less scatter when comparing the results with standard UCS tests.
- Some tests performed on saturated rock showed similar results to the ones performed on dry samples, suggesting that the saturation of the rock does not affect the results, at least on the rocks in which the saturation does not alter their structure.
- The experimental evidence shows that the specific energy can be obtained with confidence from a single scratch test.

The fact that the scratch test if performed continuously on a piece of rock and the resolution of the instrument makes possible to get a continuous log of the interval tested, instead of a single value compared to the uniaxial test.

3.2.5 Other Methods

Other methods used to estimate the UCS include Simple and Multiple Regression Equations, Models based on Fuzzy Logic Analysis, Estimation by Neural Networks, Estimations based on Evolutionary Programming and Estimation based on Regression Trees (Briševac, et al., 2016).

3.3 Motivation to Build a New Device

In the previous sections were discussed the way to measure the UCS in the laboratory and different alternative ways to estimate the UCS.

To perform UCS tests (or triaxial tests) it is necessary to extract rock cores while drilling the well. These coring operations involve many technical considerations, are time-consuming and hence, expensive. Once the cores have been obtained, the rock has to be prepared in cylindrical specimens with specific dimensions and flat, parallel ends to be able to obtain representative results. The whole process, from the extraction of cores until the final UCS results are available, can take from weeks up to months depending on the logistics and availability of laboratory installations and personnel.

Other alternative methods have shown to be accurate within certain limits and they all have limitations in their application.

If we are able to measure the properties of the rock on cuttings, the advantages are evident. The sample preparation is relatively simple and does not require special machines and procedures. After the cuttings have been collected from the shakers and washed for geological analysis at the rig site, a small amount can be used to be tested immediately and the data

collected and analysed in place. A very common sampling frequency is every 30 ft (10 m) (Knezevic, 2019) and cuttings are collected over the entire length of the well, allowing in this way to create a strength log for the whole well.

Having information about rock strength available at the rig site is a valuable asset for real-time decisions and to collect data to characterise the field for future projects.

Chapter 4 Methodology and Experimental Results

4.1 Overview

The main goals of the performed tests are:

- Proof the proposed methodology to estimate the strength of the rock by generating and processing data to find a correlation between the strength of the rock and other electrical parameters using the crusher.
- Acquire data with a vibration sensor to analyse. The information provided by the vibration sensor can be useful for further analysis. A full vibration analysis will provide meaningful information about the process that can be correlated to the strength of the rock.
- Test the functionality of the prototype, which will be used in real test conditions with different types of rocks.

The overall process is represented by the workflow shown in Figure 20:

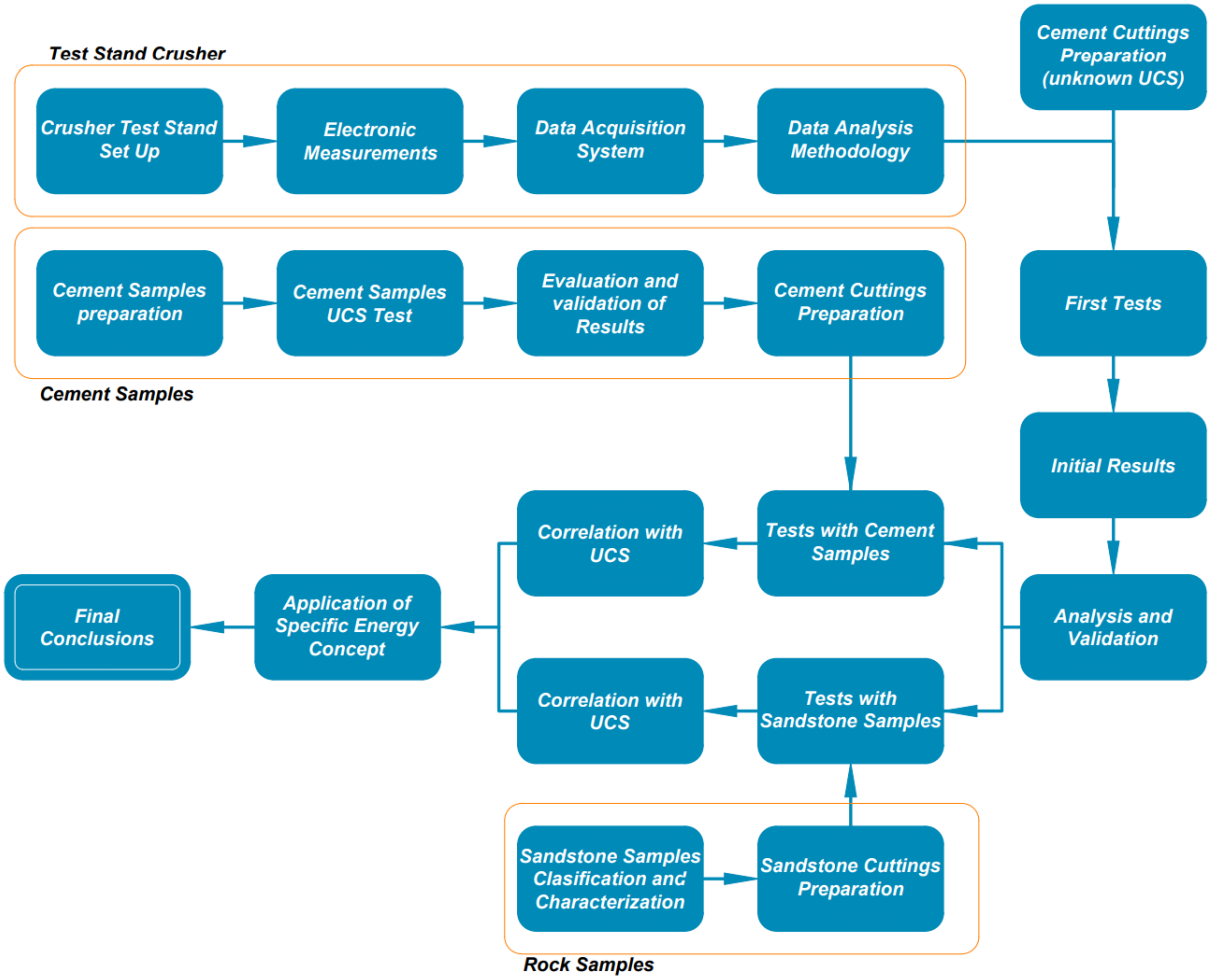

Figure 20. Overall experimental process

4.2 Sample Material

4.2.1 Cement samples

In order to have sample material with known values of UCS, several cement specimens were made to be tested in the lab. Then, cuttings were generated from the specimens and tested with the device.

The specimens of cement were prepared in cubes in the laboratory according to API Recommended Practice API-10B-2 (American Petroleum Institute, 2013) in metallic cube molds with a side length of 50 mm (Figure 21).

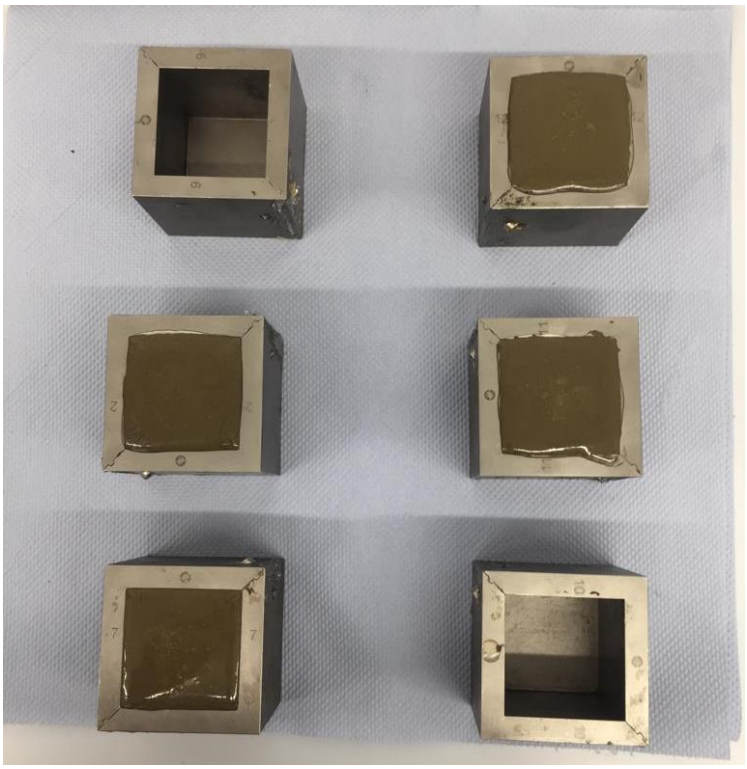

Figure 21. Preparation of specimens in cube molds.

To obtain specimens with different strength, 3 types of cement were prepared, with the following concentrations of bentonite:

- **0B** with 0% bentonite
- **4B** with 4% bentonite
- **10B** with 10% bentonite

The composition and properties of the samples are shown in Table 1:

Specimen ID	Number of Specimens	Cement mass [g]	Water		Bentonite		Measured Density [g/cm³]
			Mass [g]	%	Mass [g]	%	
0B	6	792	349	44%	0	0%	1.89
4B	5	600	360	60%	24	4%	1.71
10B	5	450	378	84%	45	10%	1.59

Table 1. Properties of the cement samples.

After the samples were cured, the upper end of each specimen was trimmed to have a flat surface, parallel to the base of the cube (Figure 22 a)

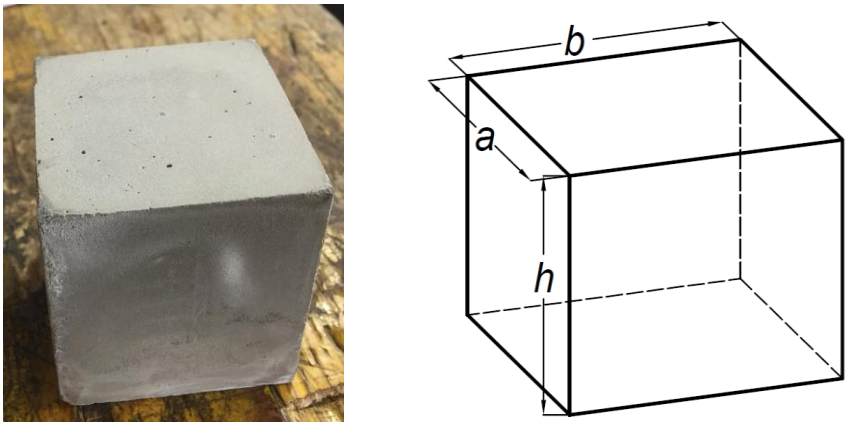

Figure 22. a) cube with trimmed end. b) dimensions of the cube (see Table 2)

A dimensional control of each specimen was performed, in order to verify that all the dimensions are within the specifications. Dimensional control is shown in Table 2:

Group	ID	Dimensions [mm]		
		a	b	h
0% Bentonite	0B1	50.7	50.7	50.2
	0B2	50.7	50.8	49.8
	0B3	50.7	50.7	50
	0B4	50.7	50.7	50.4
	0B5	50.8	50.7	49.5
	0B6	50.8	50.7	49.8
4% Bentonite	4B1	50.4	50.6	49.4
	4B2	50.5	50.5	49.15
	4B3	50.7	50.6	49.0
	4B4	50.5	50.6	49.4
	4B5	50.7	50.6	49.7
10% Bentonite	10B1	50.5	50.5	49.5
	10B2	50.4	50.4	49.3
	10B3	50.4	50.5	49.3
	10B4	50.3	50.3	49.2
	10B5	50.3	50.3	47.9

Table 2. Parameters measured in the dimensional control

4.2.2 Sandstone samples

Two specimens taken from the same sandstone, that were previously tested in the Subsurface Laboratory, (Figure 23) were also used to generate cuttings. The specimens were identified as BS-N1-3 and BS-P1. The strength of this sandstone is 50 MPa.

Figure 23. Sandstone specimens

4.2.3 Sandstone samples provided by OMV

Different samples of Nordhorn sandstones were provided by OMV. This sandstone "can be described as fine-medium-grained, porous sandstone that consists of quartz (96.6%), potassium feldspar (0.9%) and kaolinite (2.5%). The quartz grains exhibit well-developed quartz cement overgrowths (plate 1a). The kaolinite is present as cement in pore space and as replacement within potassium feldspar. Under the SEM, the kaolinite exhibits a well-developed booklet structure (plate1b). Pore space consists predominately of primary interparticle pores." (OMV, 2019)

Their strength properties were determined in the laboratory with triaxial tests. These properties are shown in Table 3:

Sample ID	Friction Angle [°]	Cohesion [MPa]
1443_Linenberg3_01	48.6	25
1443_Linenberg3_03	51.3	18.7
1443_St_Ulrich_27	45.2	37
1443_St_Ulrich_33	46.5	22.7
1443_Pionier47_10	50.5	19.8
NS Sandstone	-	-
1443_Pionier47_19	52.6	19.5

Table 3. Strength values of samples from triaxial tests.

The UCS is then calculated using the equation (7) presented in **2.4**:

$$UCS = 2 * c * \tan\left(45 + {}^{\varphi}/_{2}\right)$$

The results are shown in Table 4:

Sample ID	UCS [MPa]
1443_Linenberg3_01	132.3
1443_Linenberg3_03	106.5
1443_St_Ulrich_27	179.5
1443_St_Ulrich_33	113.8
1443_Pionier47_10	110.3
NS Sandstone	50.0
1443_Pionier47_19	115.2

Table 4. UCS Values of samples derived from triaxial tests.

A photo documentation of the samples is shown in the appendix.

4.3 Test Stand Crusher

4.3.1 Conception and Set-Up

The device consists of an electric motor connected to two rollers, which crush the cuttings of the rock that is being tested (Figure 24).

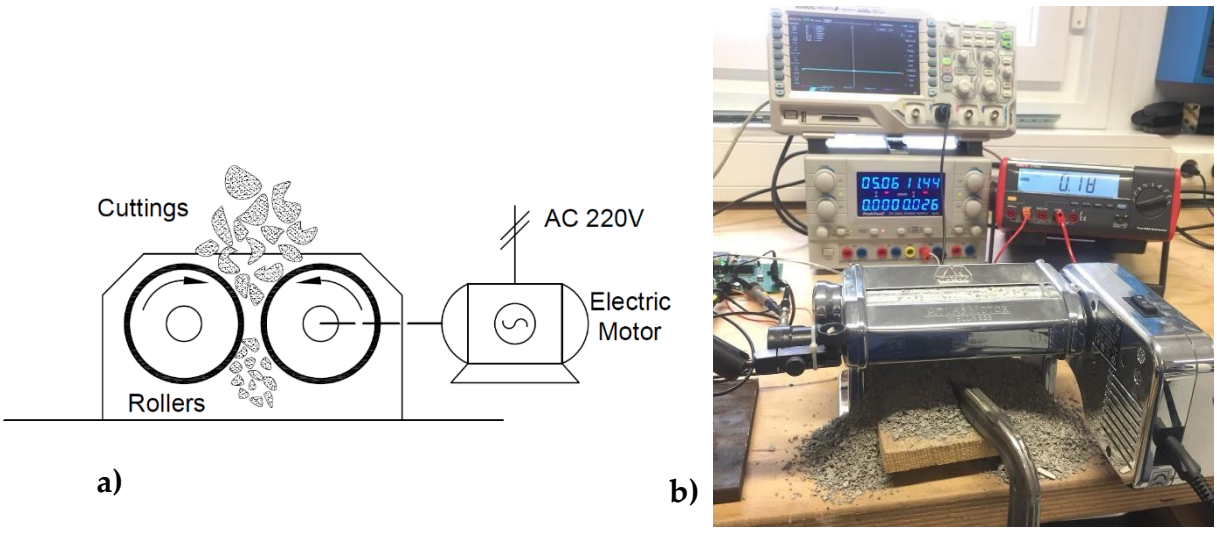

Figure 24. a) Schematic of the device. b) Actual picture of the test stand during the initial tests

Each test consists of crushing a fixed volume of 40 ml of cuttings of 4 to 8 mm in size, while measuring and recording the current of the electric motor. Then, this data generated as the current output of the motor is collected and analysed to correlate its value with the rock strength. The methodology is based on the fact that an increase in current is seen when the rock is crushed, and this increase is expected to be proportional to the UCS of the rock. The separation between the rollers is 1 mm.

A vibration sensor is also connected to the machine in order to acquire data during the crushing process.

The electric motor has the following characteristics:

Nominal Voltage: 220-240 [V]

Frequency: 50 [Hz]

Power: 100 [W]

Figure 25 shows the workflow of the data generation, acquisition and processing:

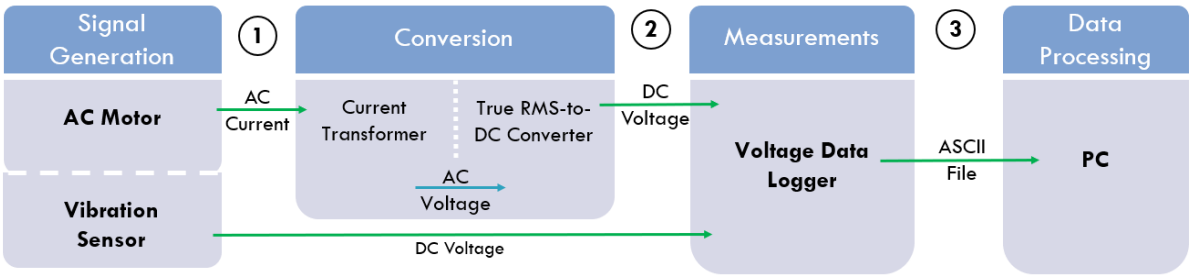

Figure 25. Data generation workflow

The current signal is measured by the current transformer, in which a voltage is induced proportional to the current that passes through it. Since the current being measured is alternate current, the voltage output is also alternate. It means that its value changes from positive to negative with the frequency of the domestic network (50_Hz). In order to get a simple numeric value of voltage independent of time, the signal is processed by a True RMS-to-DC converter.

Figure 26 shows the linear relationship between input in mA (AC) and output in mV (DC) (points 1 and 2 respectively in Figure 25).

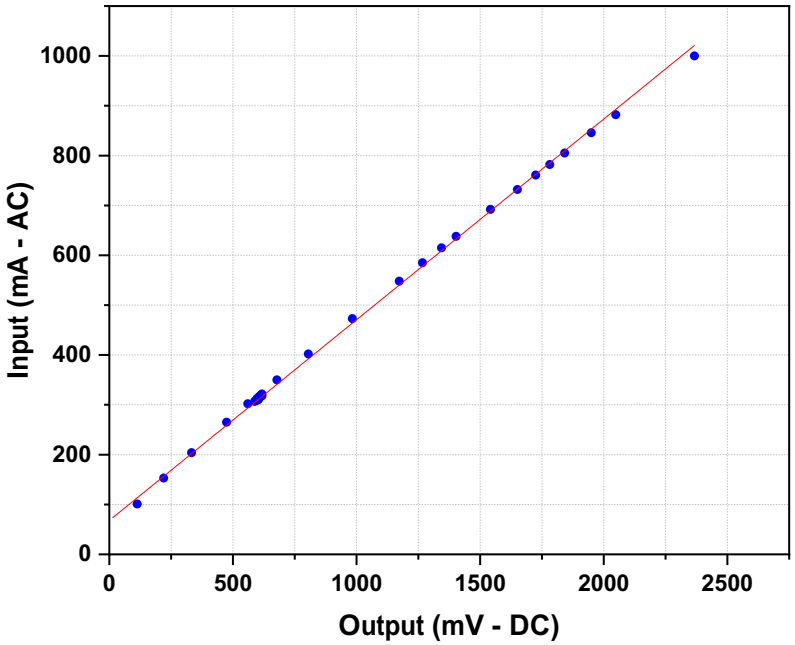

Figure 26. Conversion from mA (Alternate Current) to mV (Direct Current)

This DC voltage is measured by the data logger. This device is used to measure and record slow-moving signals over long periods of time. It can measure and record up to four channels and the signals are instantly displayed on the PC screen using a specific software (Figure 27). All the measurements are automatically stored in the memory as an ASCII file for further processing (Figure 28). The data logger can take up to 1000 samples per second. In this case, we are recording 500 samples per second, to simplify data storing and processing.

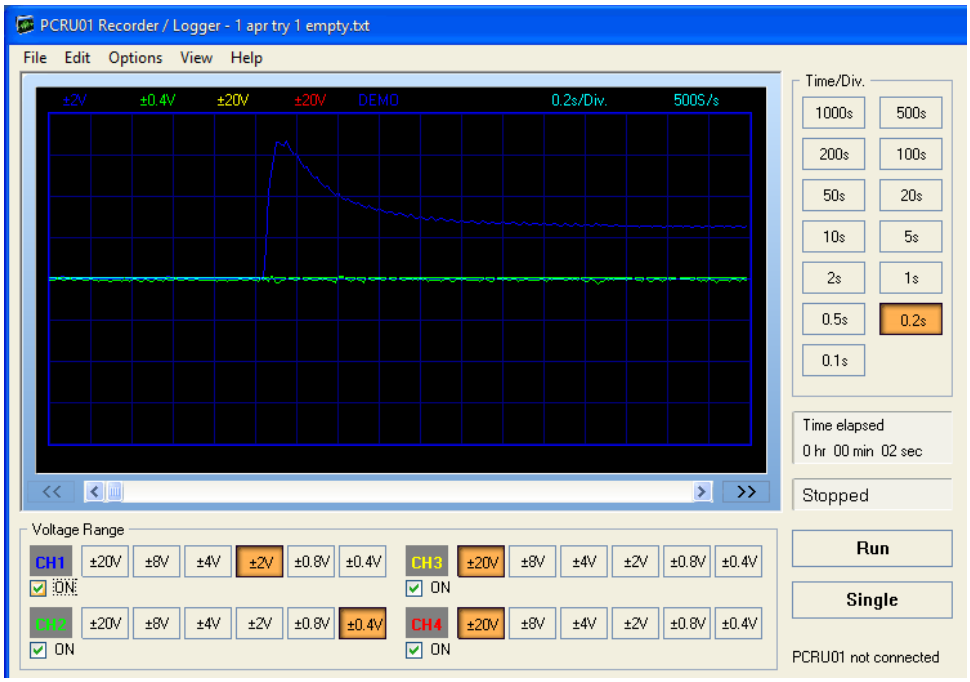

Figure 27. Screen of the Data Logger

```
START:  4/1/2019        1:37:14 PM

TIME STEP:
100 = 0.2s

VOLTAGE RANGES:
CH1: ±2V        CH3: ±20V
CH2: ±0.4V      CH4: ±20V

N       CH1     CH2     CH3     CH4     Time/s  CH1/V   CH2/V   CH3/V   CH4/V

0       515     504     515     515     0.000   0.012   -0.006  0.117   0.117
1       517     506     515     515     0.002   0.020   -0.005  0.117   0.117
2       514     512     515     515     0.004   0.008   0.000   0.117   0.117
3       515     505     515     515     0.006   0.012   -0.005  0.117   0.117
4       515     507     515     515     0.008   0.012   -0.004  0.117   0.117
5       516     506     515     515     0.010   0.016   -0.005  0.117   0.117
6       515     510     515     515     0.012   0.012   -0.002  0.117   0.117
7       515     508     515     515     0.014   0.012   -0.003  0.117   0.117
```

Figure 28. ASCII file generated by the Data Logger

Figure 29 shows a typical test curve performed on a cuttings sample. The current curve (red line) clearly describes the behavior of the electric motor during the test. At startup (point 1), the current increases generating a short duration peak called inrush current. This value can be between 5 to 10 times the nominal current of the motor. Then, the current drops to its nominal value (point 2). When the motor is loaded with cuttings (point 3), the current increases while the rollers crush the rock (between 3 and 4), since more energy is required. Once all the

cuttings are crushed, the current returns to its nominal value (point 4) until the motor is turned off (point 5).

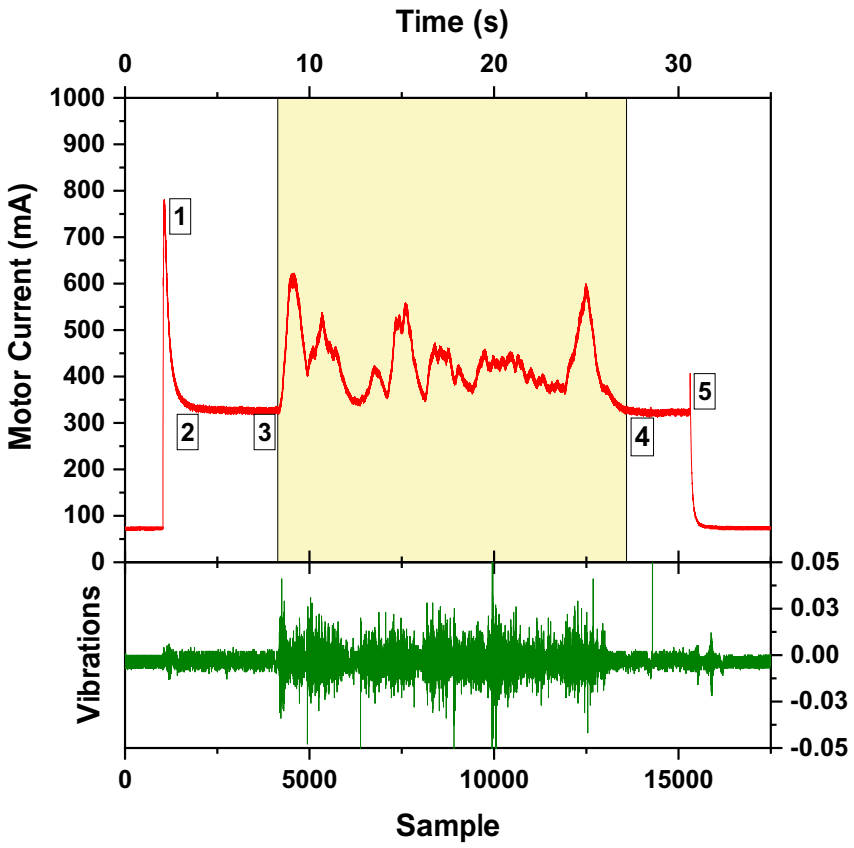

Figure 29. Load curve of a test

The output of the vibration sensor is represented by the green line in the plot. During the crushing time it can be clearly seen that the vibrations level increases. This signal is used quantitatively as complementary information of the main data source. A complete vibration analysis is not performed, as it exceeds the scope of this thesis.

In the highlighted area (between 3 and 4), a statistical analysis is performed to obtain the mean value and standard deviation of the current, which will be then used as an indicator of the rock strength.

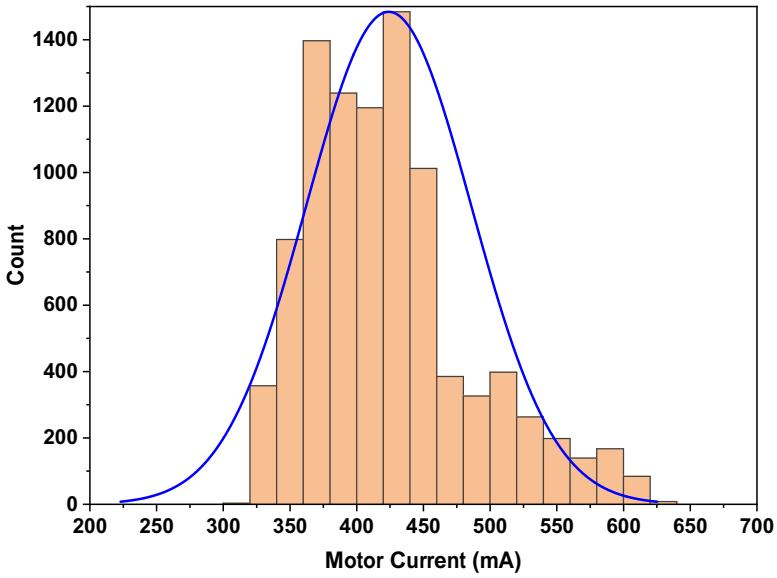

Figure 30. Statistical distribution of the current in the test zone

Figure 30 shows the distribution of the values of the current in the load area. The mean value and standard deviation are then represented in the plot as a dotted line (Figure 31).

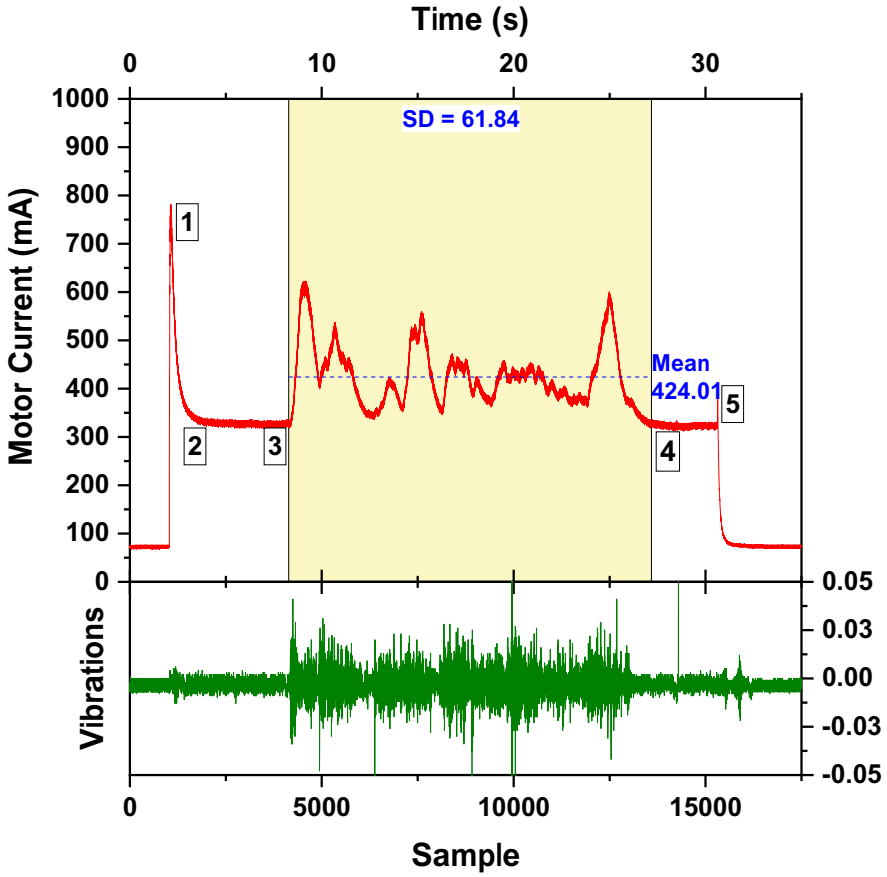

Figure 31. Load curve including Mean Value and Standard Deviation

4.3.2 Preliminary Tests

A series of preliminary tests were performed using two types of cement cuttings with different strength. Although the difference in strength was evident, the UCS value of each cement type was unknown.

Before testing the rock samples, the motor was run unloaded to determine the nominal current that is going to be used as a base for the analysis. The nominal value of the motor is 324 mA, as shown in Figure 32:

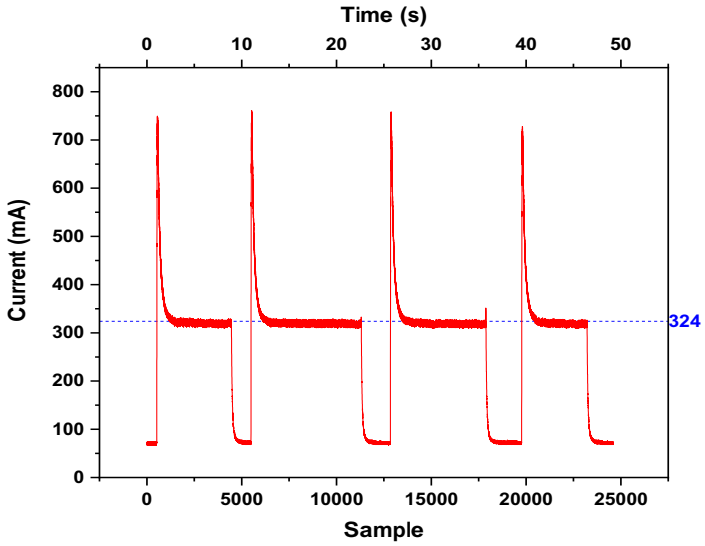

Figure 32. Calibration of the Nominal Current of the motor

The results are shown in Figure 33:

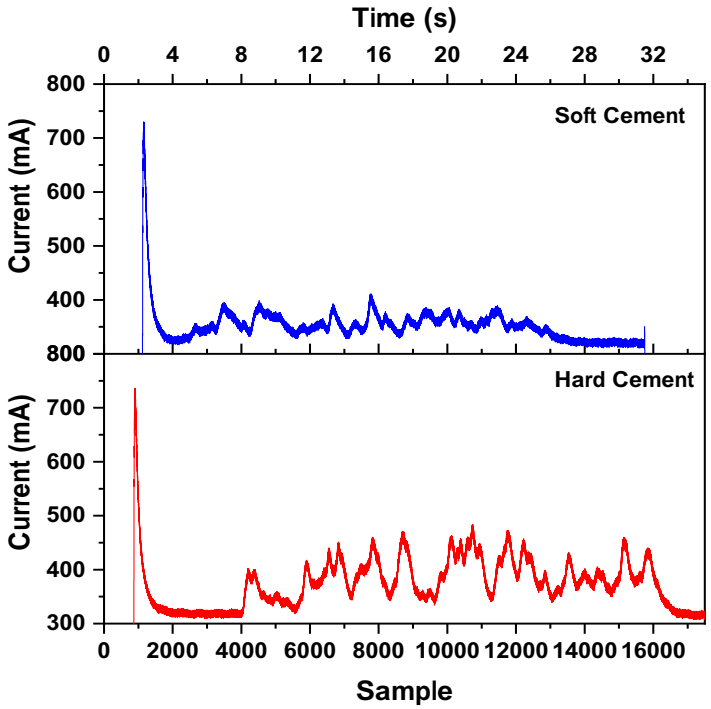

Figure 33. Result of the preliminary tests using two cement types

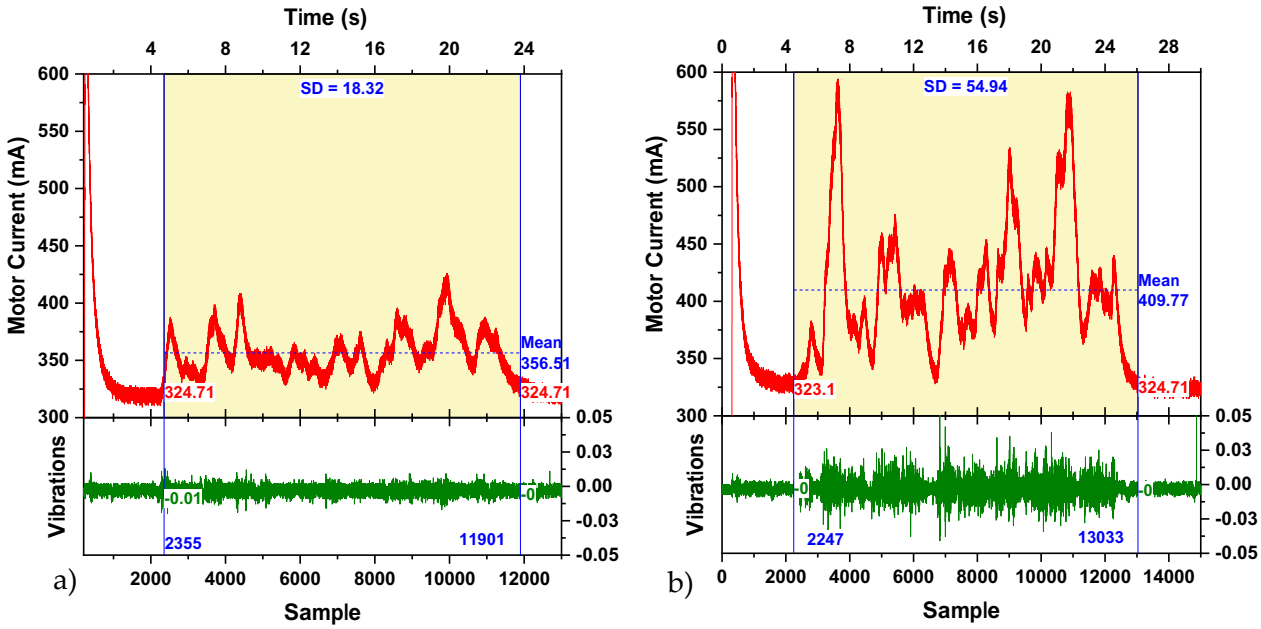

Figure 34. Test curves including statistical analysis. a) soft cement. b) hard cement

A total of six tests were performed and they showed consistency in the current mean value for each type of cement, as shown in Figure 35. The error bars represent the standard deviation. The horizontal dotted line at 324 mA represents the nominal current of the motor.

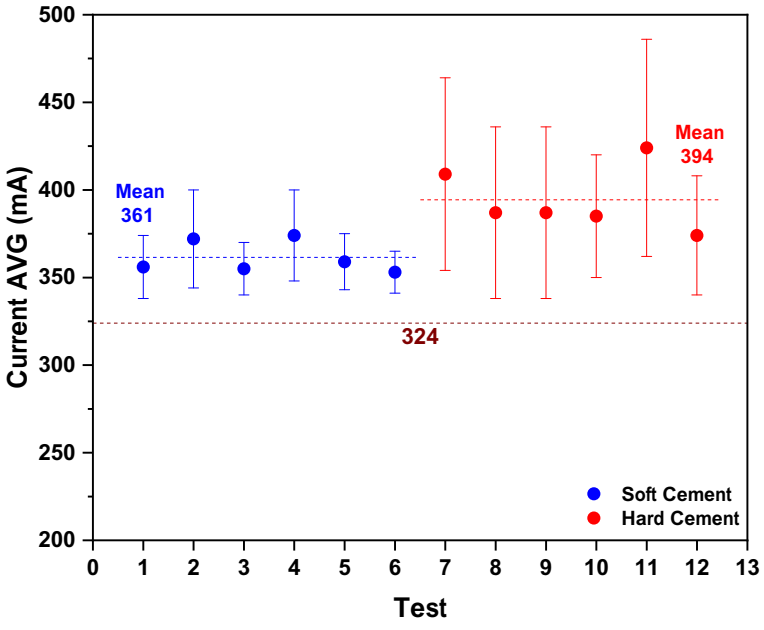

Figure 35. Preliminary test results

By analysing the data from these tests, we can make some initial observations:

1. The mean current of the soft cement tests is clearly lower than the one of the hard cement tests.

2. The values of the current have more dispersion in the case of the hard cement, compared with the soft cement.

As the values of strength of each cement type are unknown, a calibration is necessary in order to correlate the strength values of the rock with the mean value of the current.

4.3.3 Performed Measurements

Using the cuttings generated from the previously tested specimens, a series of 13 tests were performed for each type of cement (0B, 4B and 10B).

The next figures show a test of each type of cement along with the histogram of frequency of the current.

0B - Test 1

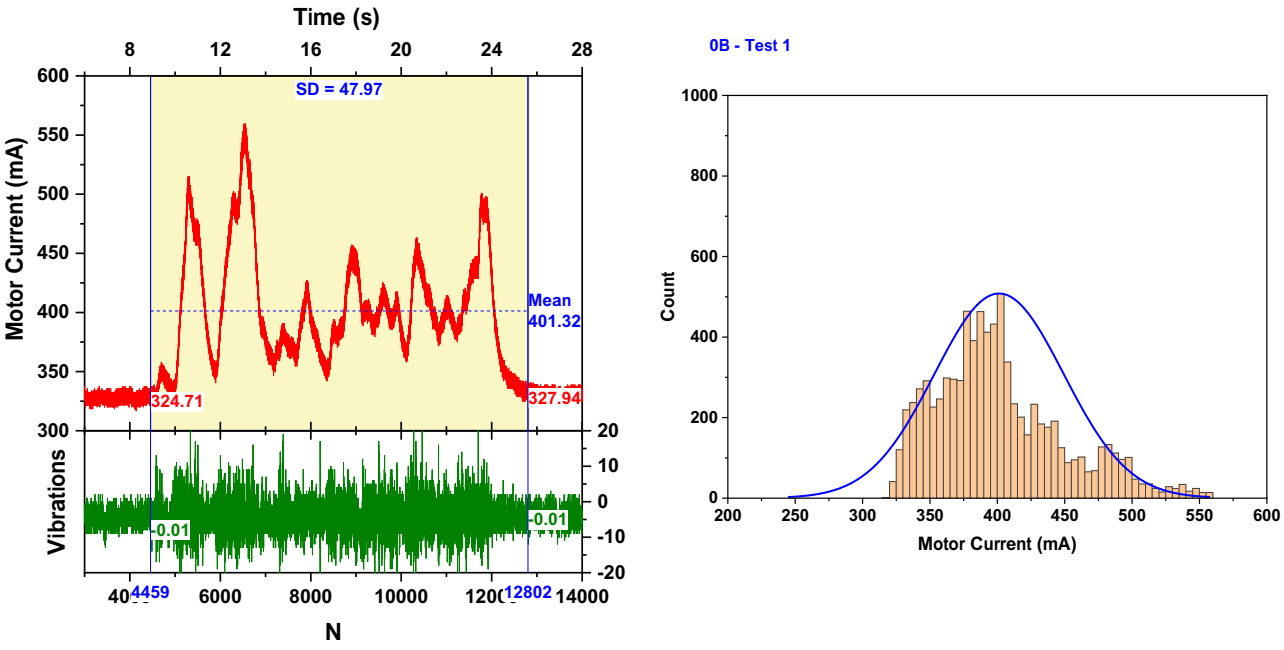

Figure 36. Test curve and histogram of frequencies of the 0B sample.

4B - Test 1

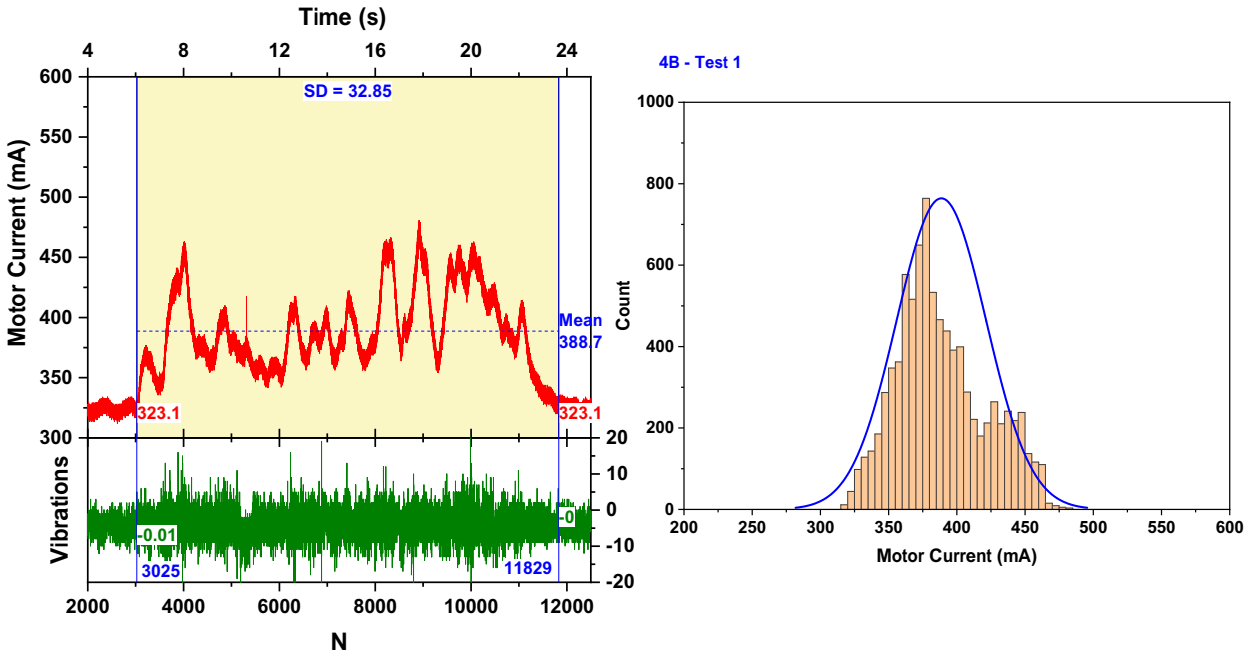

Figure 37. Test curve and histogram of frequencies of the 4B sample.

10B -Test 1

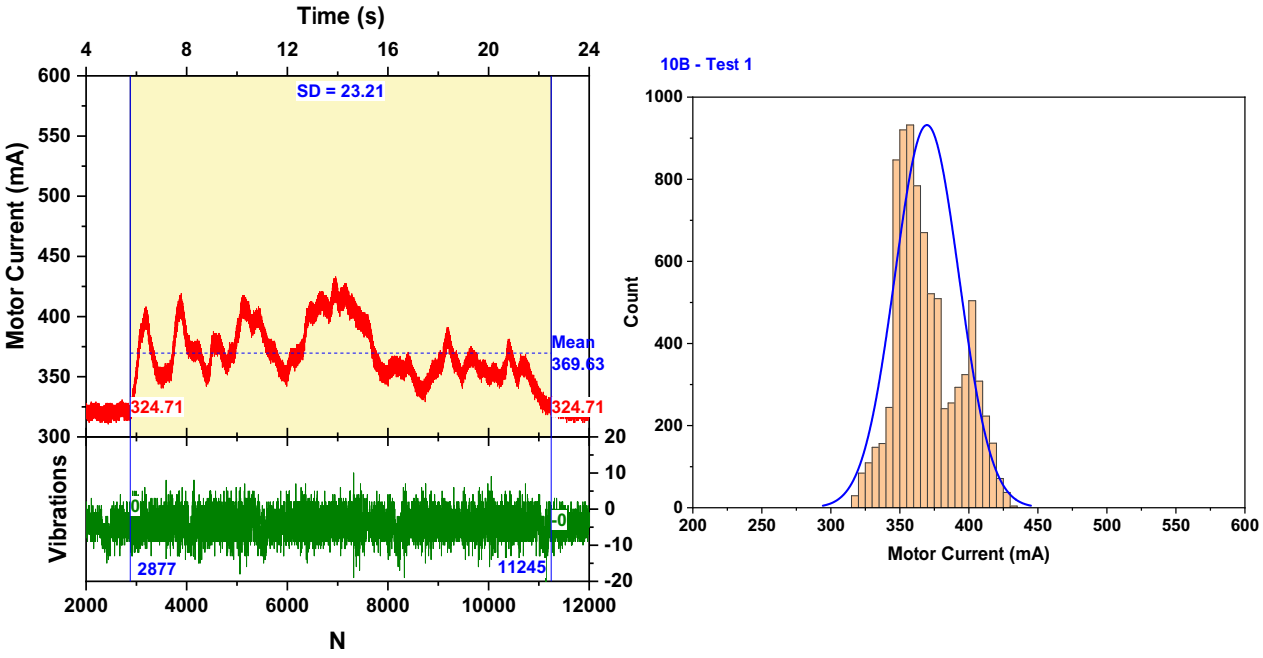

Figure 38. Test curve and histogram of frequencies of the 10B sample.

The load curves of the group 0B show in general a sharper shape than the curves of the group 4B and 10B, respectively. This might be due to the higher brittleness character of the cement with higher strength.

Results are tabulated in Table 5:

Test Number	Current (mA)		
	0B	4B	10B
1	401	389	370
2	414	378	365
3	395	398	373
4	395	390	363
5	383	383	373
6	393	392	378
7	414	387	374
8	392	396	398
9	401	400	387
10	394	389	377
11	373	391	404
12	385	395	382
13	383	381	398

Table 5. Test results for each group of material

4.4 UCS Test stand

4.4.1 Conception and Set-Up

The UCS test stand consists of a Bench Press Carver Model M 3853 as shown in Figure 39.

Specifications of the press:

- Manually operated
- Clamping force 25 tons
- Daylight opening 0.75" – 16" (Factory set at 6-1/2")
- Stroke 6-1/2"
- Two (2) fully threaded columns
- 9" x 9" work area
- 0-50,000 lb Analog pressure gauge, reading in 500 lb increments (digital gauge also available)
- Light grey safety shield
- Dark grey frame
- Dimensions: 19"L-R x 24"F-B x 42"H
- Weight: 350 pounds

Figure 39 . Load Frame used to perform the UCS tests

4.4.2 Performed Measurements

A series of 16 UCS test in the press were performed in accordance with API Recommended Practice API-10B-2 (American Petroleum Institute, 2013). The destroyed specimens after each test (Figure 40) were stored to make the cuttings to be tested in the Crusher

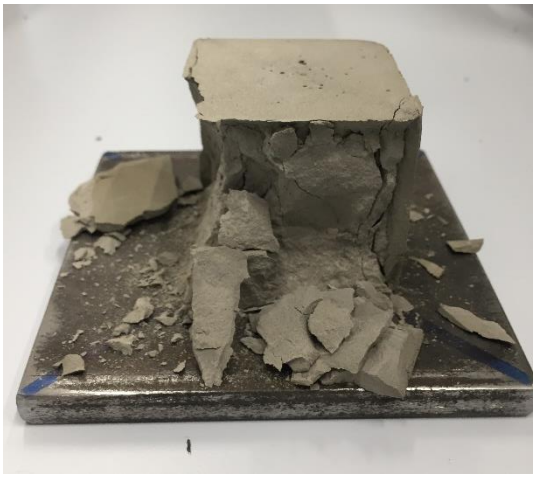

Figure 40. Cement specimen after UCS test.

The results of the tests are shown in Table 6:

Group	Specimen ID	Force [metric Tons]	UCS [MPa]
0 % Bentonite	0B1	9.07	36.3
	0B2	7.26	29.0
	0B3	7.48	29.9
	0B4	7.03	28.1
	0B5	7.71	30.8
	0B6	6.58	26.3
4 % Bentonite	4B1	4.99	20.0
	4B2	4.99	20.0
	4B3	4.99	20.0
	4B4	6.12	24.5
	4B5	4.76	19.1
10 % Bentonite	10B1	2.49	10.0
	10B2	2.95	11.8
	10B3	2.95	11.8
	10B4	3.63	14.5
	10B5	3.86	15.4

Table 6. Results of UCS tests performed on cement specimens

4.5 Results and Discussion

4.5.1 UCS Tests

The values from Table 6 are represented in Figure 41:

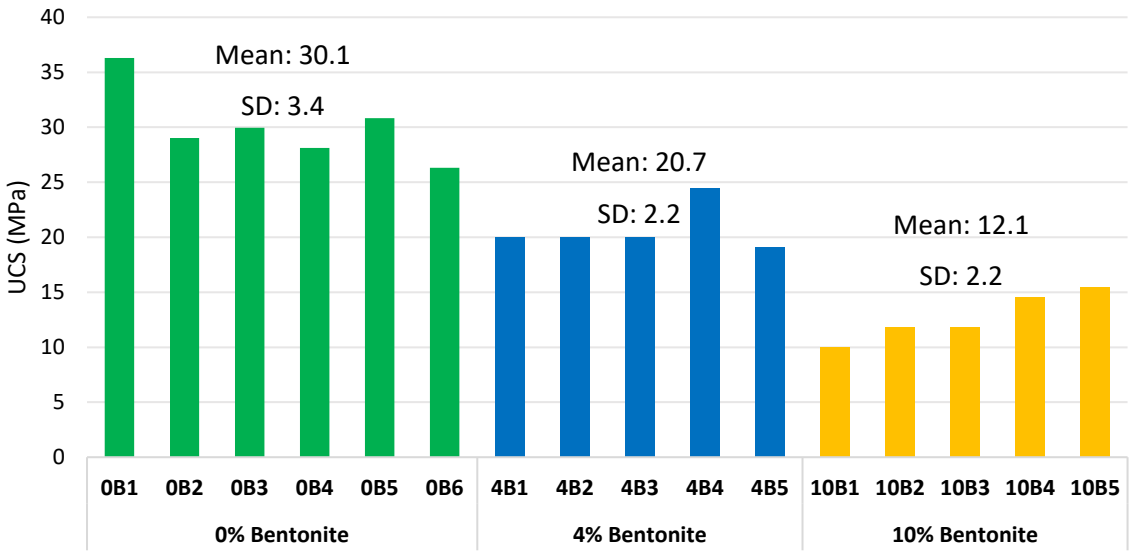

Figure 41. Graphical representation of UCS tests for each group of cement

As expected, the addition of bentonite has a strong impact on the strength of the cement, with a reduction of strength as the percentage of bentonite increases. All the UCS tests show consistent values with considerably low dispersion.

4.5.2 Test Stand Crusher

The histograms show in general a Bimodal shape (Goos, 2015) suggesting that there might be two processes involved in crushing the rock. It is important to highlight that the peaks on the histograms are rather erratic and do not follow a pattern. Sometimes the smaller peak represents a higher current and sometimes a lower current, compared with the mean current (Figure 42).

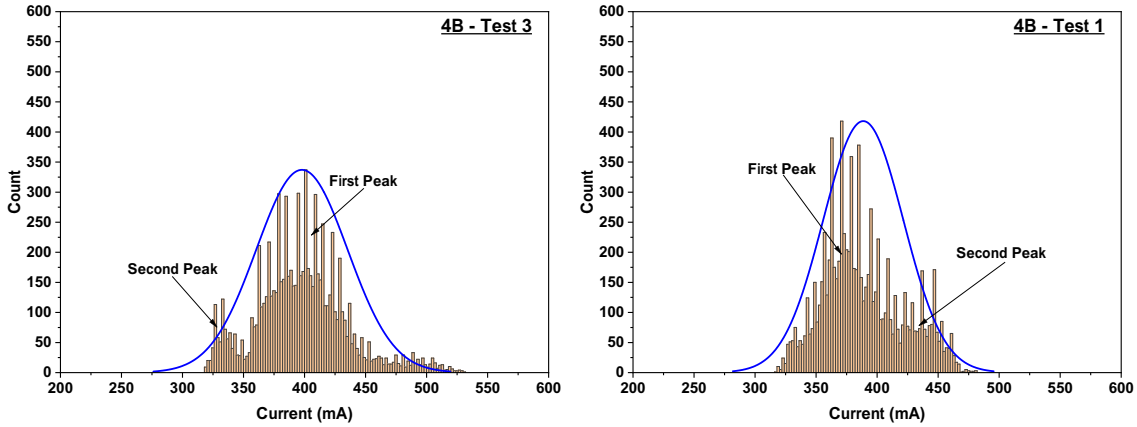

Figure 42. Bimodal character of the current histograms

Figure 43 shows all the results of the mean of the current for each type of cement:

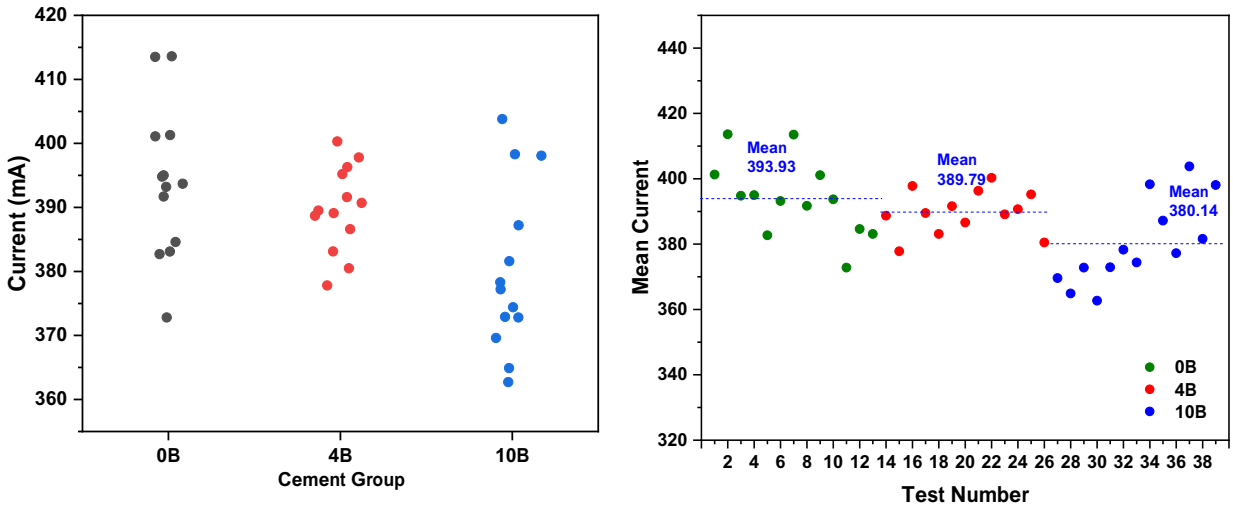

Figure 43. Test results using the mean of the current as a strength indicator. a) by group of cement type. b) by test number.

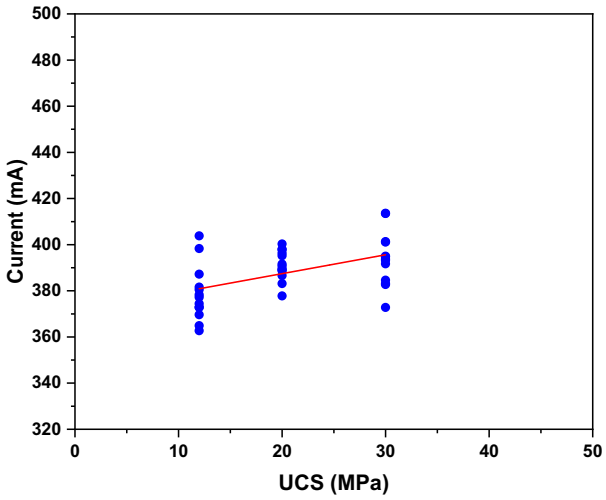

Figure 44. Correlation between the main current and UCS of the tested material.

The first plot shows the results by groups, and the dispersion in values is quite high, with a variation coefficient of 2.9%, 1.7% and 3.9% for 0B, 4B and 10B respectively.

Analysing Figure 44, we can see that there is a relationship between the strength of the rock and the mean current of each test, although this linear relationship is not really strong.

We can use the mean value of tests for each group as an indicator of the strength, taking as a base for the analysis the mean value of the less strong material (10B). As we can see in Figure 45, the difference in strength is given by the current 16.4% higher (4B) and 22.9% (0B).

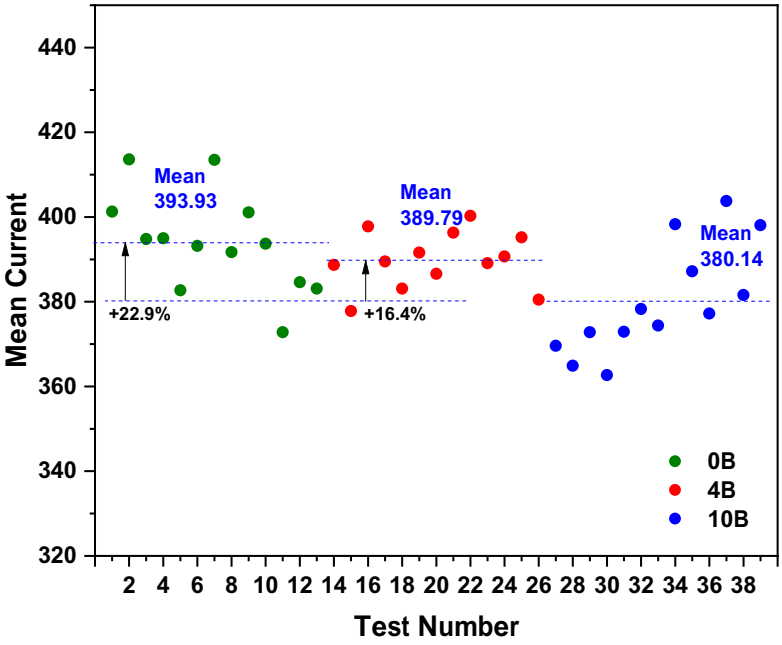

Figure 45. difference in rock strength expressed as a percentage

The Pearson's square of the linear fit is 0.5. This might be because we are not considering the time in this calculation, which is a very important parameter in the process as it takes longer for a hard material to be crushed.

4.5.3 Factors affecting the measurements

- Cuttings size: it is evident that the size of the cuttings changes the values of current required to crush the cuttings, as the torque required is higher when the cuttings are bigger.
- Separation of the rollers: in the same way as the size of cuttings, the separations of the rollers has a big impact on the energy required.
  In both cases, no tests were performed to see the influence of these factors. In the course of the design of the prototype, several factors had to be kept constant to be able to perform the tests.
- Feeding system: currently the cuttings are fed into the machine manually, which influences the speed of the cuttings being crushed. Although with the introduction of the concept of Specific Energy its influence is minimized, the impact still exists and needs to be addressed.
- Homogeneity of the material: here are presented only the results of tests performed on cuttings samples made from cement and sandstones, and the results show differences between the two materials, suggesting that the homogeneity has an influence on the results.

4.6 Analysing results in Terms of Specific Energy

4.6.1 Concept of Specific Energy

The concept of Specific Energy was developed by Teale (1966) for drilling engineering, serving as a basis for further work in the area of drilling optimization.

Several research papers (Dupriest and Koederitz, 2005; Pessier, 1992; Waughman et al., 2002) show the successful application of this concept to assess and optimize the drilling process using real field data, showing the advantages of this method.

Detournay et al. (1996) used the concept of Specific Energy in the design of the Rock Strength Device (SRD).

If we apply the same concept to our device, the power consumption of the device (electric motor + rollers) can be expressed as follows:

$$P = U * I \tag{8}$$

Where

$P = power, expressed\ in\ Watts$

$U = nominal\ voltage, expressed\ in\ Volts$

$I = current, expressed\ in\ Amps$

and the energy is obtained by multiplying power by time, thus:

$$E = P * t = U * I * t \tag{9}$$

In our case, as the current changes over time, the expression of the energy becomes:

$$E = U * \left[\int_{ts}^{te} I(t)dt\right] \tag{10}$$

Where the integral in brackets represents the area below the load curve of each test. ts and te represent the start and end time of the test, respectively.

Finally, to obtain the specific energy (SE) that is consumed by the device to crush a certain volume of rock, the expression is divided by the volume of rock V_r and the overall efficiency of the device η:

$$SE = \frac{U}{\eta * V_r} * \left[\int_{ts}^{te} I(t)dt\right] \tag{11}$$

The Specific Energy is commonly expressed in J/cm^3, which is equivalent to MPa and is more convenient for us to correlate with the strength of the rock.

In our case:

$U = 220\ [V]$

$V_r = 40\ [ml]$

$\eta\ is\ assumed\ to\ be\ 0.96$[1]

Rearranging the equation (4):

$$SE\ [MPa] = \int_{ts}^{te} [5.73 * I(t)dt] \tag{12}$$

It means that multiplying the load curve of the test by $\frac{U}{\eta * V_r}$, the new curve represents the specific power in MW/m^3. The shape of the curve remains the same, as it is only affected by a

[1] This value is assumed, as the determination of the overall efficiency of the device exceeds the scope of this work.

constant. After the integration, the area below the curve (in light blue) represents the specific energy in MPa:

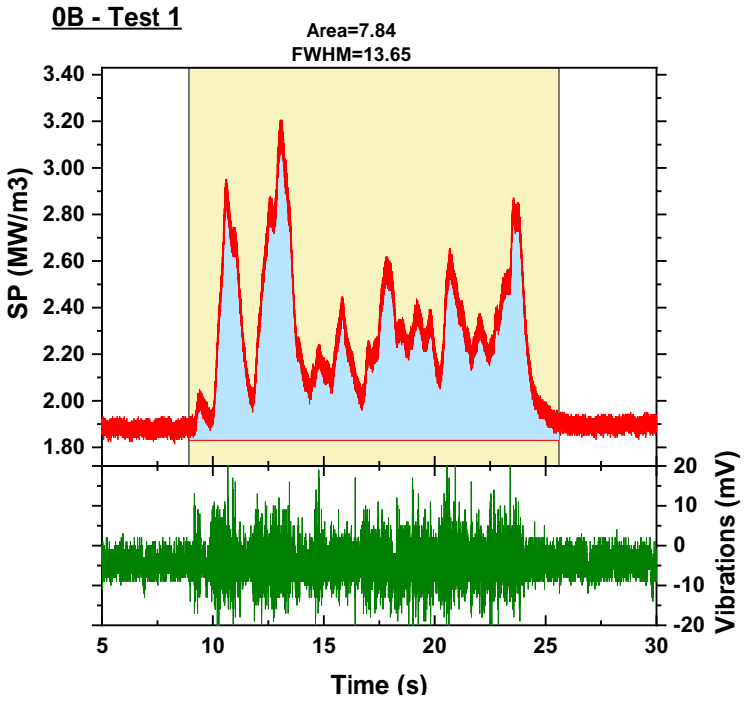

Figure 46. The light blue area represents the Specific energy of the test

The calculated value of the Specific Energy is shown on top of on each plot, along with the Full Width at Half Maximum (FWHM), which in our case does not have any practical use.

4.6.2 Results and Discussion

All the ASCII data files from the tests done are stored in the CD attached to this thesis.

The results using the new approach are shown in Table 7:

Test Number	Specific Energy (MPa)		
	0B	4B	10B
1	7.84	7	7.4
2	11.23	6.36	5.02
3	9.43	7.56	6.03
4	8.86	8.33	5.07
5	7.32	7.39	6.05
6	8.63	8.43	6.84
7	10.42	7.92	8.46
8	9.51	8.53	7.03
9	9.51	9.31	6.63
10	9.39	8.5	6.27
11	10.09	8.72	7.79
12	8.71	9.05	5.98
13	9.82	7.42	7.05

Table 7. Results of the tests using the concept of Specific Energy

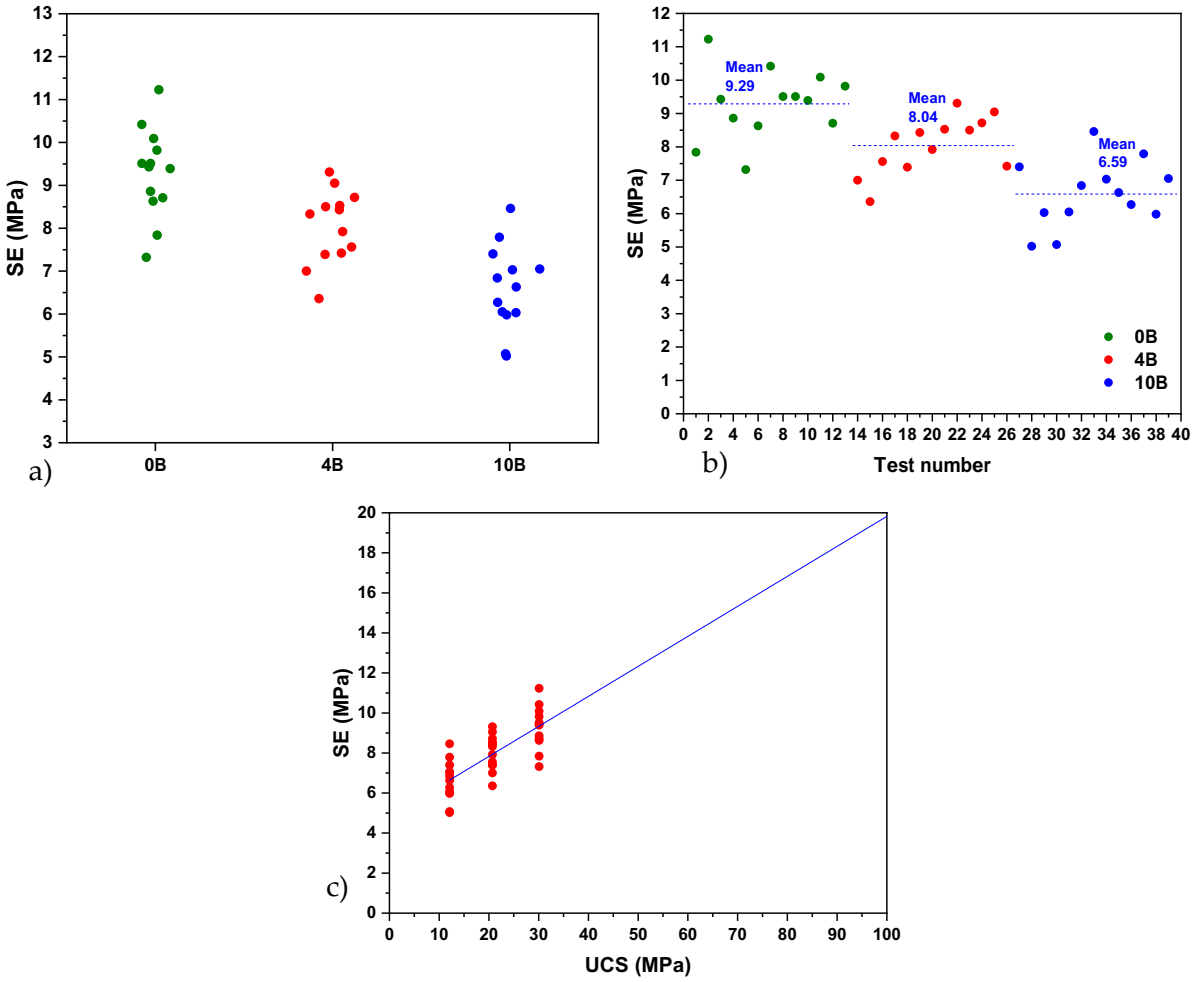

Figure 47. Test results using the concept of Specific Energy. a) by group of cement type. b) by test number. c) correlation between specific energy and UCS of the tested material.

The results show now less scatter in values for each group of cement (Figure 47 a)).

Also, it is very important to highlight that using these new results, it is easier to differentiate the materials with different hardness, comparing with the current as an indicator. As we can see in Figure 47 b), the difference in the mean value of each group is bigger and more noticeable. It can be used as a better indicator of the rock strength, as it expresses better the difference in percentage as shown in Figure 48.

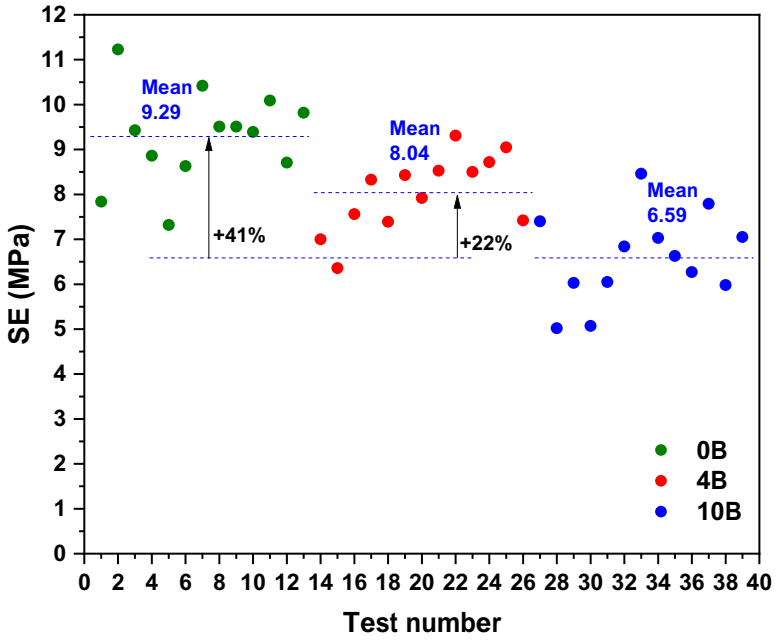

Figure 48. Difference in rock strength expressed as a percentage

In Figure 47 c), a better linear correlation is shown between UCS and SE, with a Pearson's r value of 0.76, which can be considered as a good fit.

Finally, the different rock types, described in **4.2.3,** were tested using the concept of Specific Energy and the results are shown in Figure 49:

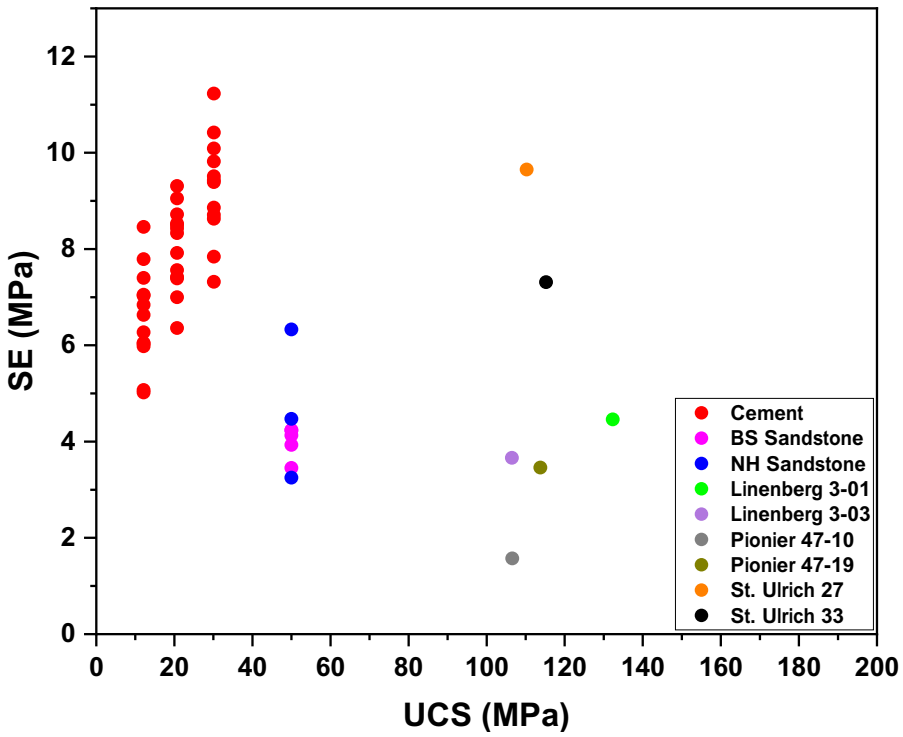

Figure 49. Final results including sandstone samples

In this plot we can clearly see that the tests performed on cement samples have a very good correlation between UCS and SE, but it is not the case of rocks samples. In the second case, for some samples with higher UCS values the SE is lower than cement samples. This might be due to a scale issue, where the grain size and cementation of the rock take a more important role.

4.6.1 Conclusions

It is evident that the correlation of UCS and SE of cement samples is good as the cement does not have predominant grains; it is a homogeneous material with the same properties in the whole body.

Unlike the cement, the sandstones tested here are composed of grains of minerals and a cementing material between the grains that holds them together and may be composed of a matrix of silt or clay-size particles that fill the space between the grains (King, 2019).

This difference in materials is appreciated in Figure 50.

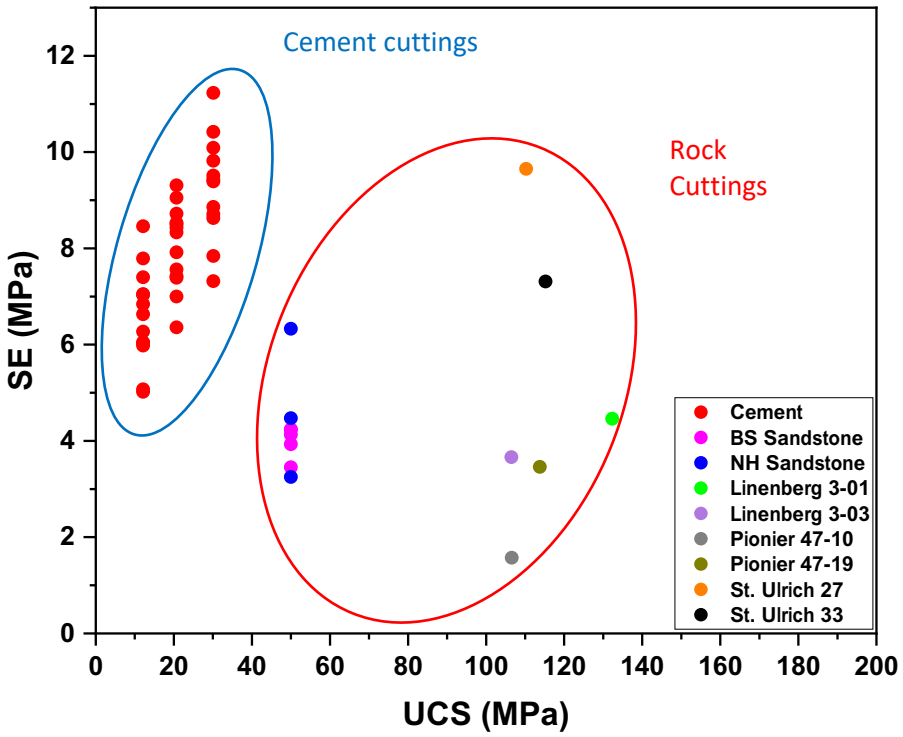

Figure 50. Differences in Specific Energy for cement and rock.

Although the UCS of both materials is the same (macro scale), there is a difference in the Specific Energy required to crush a rock, since in a small scale (cuttings) the grain size and the cementing material acquire more importance in the crushing process. As mentioned in 4.3.1, the separation between rollers is 1 mm which means that after the cuttings pass through the crusher, the grains are not together anymore and the bonds created by the cementing material are broken.

Cohesion is the strength of bonding between particles (Kearey, 2001) and in this case we can assume that is the representative parameter that can be correlated to the Specific Energy in the crusher.

We can plot Specific Energy vs Cohesion, for those samples that have been tested in a triaxial cell and cohesion was determined:

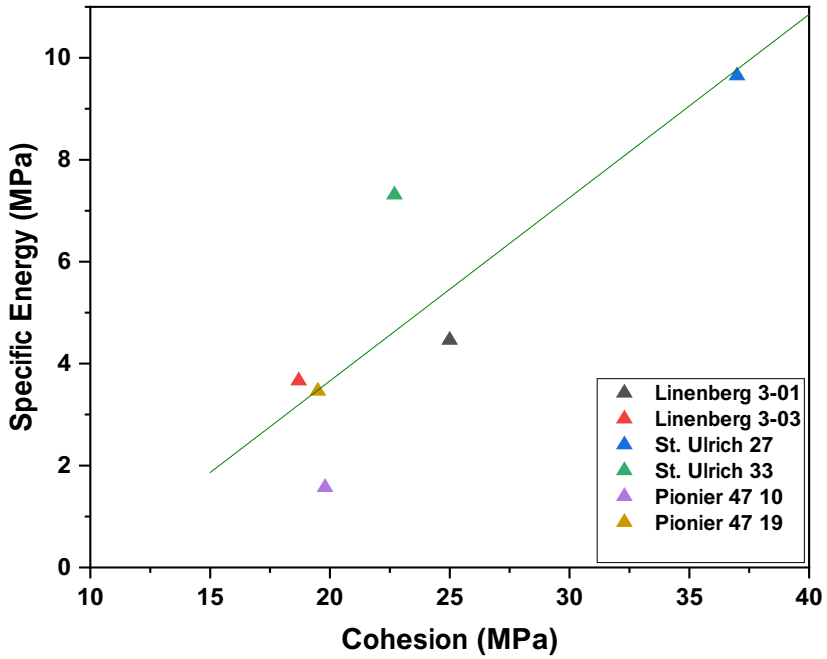

Figure 51. Correlation between Specific Energy and Cohesion

The plot (Figure 51) shows a linear correlation between Cohesion and Specific Energy, giving initial experimental evidence to support the assumption that the cohesion of the rock is the main parameter controlling the crushing process of small pieces of rock.

Although the experiments with real rock cuttings showed inconsistencies in the correlation of UCS and Specific Energy, using the Cohesion instead of the UCS provides better results and meaningful information about the rock being tested. This means that using the crusher we are able to derive values of the Cohesion of the rock, not UCS. This is more reasonable, due to the fact that the crushing process taking place in the rollers destroys the cementing material between the grains of the rock, rather than compressing the rock until failure as during a UCS test.

This correlation is important for drilling engineering, since the drilling process using rotary drilling bits is mostly a grinding action that breaks apart the rock pieces (Bourgoyne Jr. et al., 1986), which is a process similar in nature to the one that happens in the crusher. This correlation can be used as an index for ROP prediction and optimization.

In order to better understand this conclusion and to confirm these initial results, more detailed and deeper tests need to be carried out.

4.7 Future Work

For the further development of the Crusher and methodology, the following points are recommended:

Crusher. A sturdy device needs to be developed to test high strength rocks. The prototype showed the applicability of the methodology to test different types of rocks; but has some limitations regarding the maximum strength that it can withstand. Based on the original prototype, some improvements are necessary such as mechanical structure, bearings design, gears, shafts and rollers.

Electronics. General improvement in the electronic conversion and acquisition systems will provide a better signal to process. Although the signal has now very good quality, it can be improved. Using a Data Logger with a higher vertical resolution will give us the possibility to measure current a higher range of values.

Feeding system. The implementation of a feeding system is necessary to feed the cuttings into the crusher in an automated way. This will reduce the scatter in the data generated, and the load curve should be smoother.

Automated data processing methodology. It is possible to perform automated data acquisition and analysis in real-time using LabView and Origin. LabView is used as the interface between the data logger and the PC. It also controls the data acquisition that is then sent to Origin for further processing. Using standard templates in Origin for automated processing makes the tests easier and reduces processing work.

Vibration analysis. As one purpose of the performed test was to collect vibration data, further investigation is necessary to obtain information about the crushing process and the properties of the crushed rocks.

Extensive Test Campaign. It is recommended to perform an extensive testing campaign using different types of rocks with different strength to evaluate results and test the crusher in a wider range. This will provide a better correlation of parameters and they can be classified according to the different types of rocks.

During this first stage of the development, that is the subject of this thesis, many parameters were fixed in order to perform the tests. It is necessary to continue studying the influence of the different factors affecting the measurements. Cuttings size is one of the most important factors that need to be assessed, since cuttings between 4 to 8 mm in size are not always available during drilling operations.

Bibliography

Afsari, M., Ghafoori, M., Roostaeian, M., Haghshenas, A., Ataei, A., Masoudi, R., 2009. Mechanical Earth Model (MEM): An Effective Tool for Borehole Stability Analysis and Managed Pressure Drilling (Case Study), in: SPE Middle East Oil and Gas Show and Conference. Presented at the SPE Middle East Oil and Gas Show and Conference, Society of Petroleum Engineers, Manama, Bahrain. https://doi.org/10.2118/118780-MS

Amani, A., Shahbazi, K., 2013. Prediction of Rock Strength using Drilling Data and Sonic Logs. International Journal of Computer Applications 81, 5–10. https://doi.org/10.5120/13982-1986

American Petroleum Institute, 2013. API Recommended Practice B-2 - Recommended Practice for Testing Well Cements.

Bourgoyne Jr., A.T., Chenevert, Ma.E., Millheim, K.K., Young Jr., F.S., 1986. Applied Drilling Engineering, 1st ed, SPE Textbook Series. Richardson, Texas.

Briševac, Z., Hrženjak, P., Buljan, R., 2016. Models for Estimating Uniaxial Compressive Strength and Elastic Modulus.

Chang, C., Zoback, M.D., Khaksar, A., 2006. Empirical relations between rock strength and physical properties in sedimentary rocks. Journal of Petroleum Science and Engineering 51, 223–237.

Detournay, E., Drescher, A., Adachi, J., 1996. Determination of rock Strength Parameters from Cutting Tests. Presented at the 2nd North American Rock Mechanics Symposium, American Rock Mechanics Association, Montreal, Quebec, Canada.

Detournay, E., Drescher, A., Hultman, D., 1997. Portable Rock Strength Evaluation Device. 5670711.

Dupriest, F.E., Koederitz, W.L., 2005. Maximizing Drill Rates with Real-Time Surveillance of Mechanical Specific Energy. Presented at the SPE/IADC Drilling Conference, SPE/IADC, Amsterdam, The Netherlands, p. 10.

Goos, P., 2015. Statistics with JMP: Graphs, Descriptive Statistics, and Probability, 1st ed. John Wiley & Sons, Ltd, United Kingdom.

Hudson, J.A., Harrison, J.P., 1997. Engineering rock mechanics: an introduction to the principles, 1st ed. ed. Pergamon, Tarrytown, NY.

Kearey, P., 2001. Dictionary of Geology, 2nd ed. Penguin Group, London, England.

King, H.M., 2019. Geology.com [WWW Document]. URL https://geology.com/rocks/sandstone.shtml (accessed 7.9.19).

Knezevic, R.-N., 2019. Meeting with OMV representatives.

OMV, 2019. Description of Nordhorn Sandstones.

Pessier, F., 1992. Quantifying Common Drilling Problems With Mechanical Specific Energy and a Bit-Specific Coefficient of Sliding Friction. Presented at the 67th Annual Technical Conference and Exhibition of the Society of Petroleum Engineers, SPE, Washington, DC, USA, p. 16.

Plumb, R., Edwards, S., Pidcock, G., Lee, D., Stace, B., 2000. The Mechanical Earth Model Concept and Its Application to High-Risk Well Construction Projects. Presented at the IADC/SPE Drilling Conference, IADC/SPE, New Orleans, Louisiana, USA, p. 13.

Richard, T., Dagrain, F., Poyol, E., Detournay, E., 2012. Rock strength determination from scratch tests. Engineering Geology 147–148, 91–100. https://doi.org/10.1016/j.enggeo.2012.07.011

Santarelli, F.J., Marsala, A.F., Brignoli, M., Rossi, E., Bona, N., 1998. Formation Evaluation From Logging on Cuttings. SPE Reservoir Evaluation & Engineering 1, 238–244. https://doi.org/10.2118/36851-PA

Santarelli, F.J., University of Bologna, Civolani, L., Zausa, F., 1997. Real-Time Wellbore Stability Analysis at the Rig Site. Presented at the SPE/IADC Drilling Conference, SPE/IADC, Amsterdam, The Netherlands.

Schön, J.H., 2015. Physical properties of rocks: fundamentals and principles of petrophysics, 2nd. ed. ed, Developments in petroleum science. Elsevier, Amsterdam.

Teale, R., 1965. The Concept of Specific Energy in Rock Drilling. International Journal of Rock Mechanics and Mining Science 2, 57–73.

Tiab, D., Donaldson, E.C., 2012. Petrophysics: theory and practice of measuring reservoir rock and fluid transport properties, 3rd ed. ed. Gulf Professional Pub, Amsterdam ; Boston.

Uboldi, V., Civolani, L., Zausa, F., 1999. Rock Strength Measurements on Cuttings as Input Data for Optimizing Drill Bit Selection. Presented at the SPE Annual Technical Conferenc, Houston, Texas.

Waughman, R.J., Kenner, J.V., Moore, R.A., 2002. Real-Time Specific Energy Monitoring Reveals Drilling Inefficiency and Enhances the Understanding of When to Pull Worn PDC Bits. Presented at the IADC/SPE Drilling Conference, Dallas, TX, USA, p. 14.

Zoback, M.D., 2007. Reservoir geomechanics. Cambridge University Press, Cambridge.

Acronyms

ROP	Rate of Penetration
UCS	Unconfined Compressive Strength
MEM	Mechanical Earth Model
3D	Three-dimensional
ASTM	American Society for Testing and Materials
API	American Petroleum Institute
AC	Alternate Current
DC	Direct Current
PC	Personal Computer
ASCII	American Standard Code for Information Interchange
SD	Standard Deviation
FWHM	Full Width at Half Maximum
CD	Compact Disc
SE	Specific Energy

Symbols

g	gravitational acceleration	$\left[{}^{m}/_{s^2}\right]$
ρ	density	$\left[{}^{kg}/_{m^3}\right]$
z	depth	$[m]$
σ_h	Horizontal stress	$[Pa]$
υ	Poisson's modulus	$-$
E	Young's modulus	$[MPa]$
ε	strain	$-$
r	radius	$[m]$
l	length	$[m]$
τ	shear stress	$[Pa]$
C	cohesion	$[MPa]$
σ_n	normal stress	$[Pa]$
φ	friction angle	$[°]$
v_p	compressional wave velocity	$\left[{}^{ft}/_{s}\right]$
Δt	slowness	$[\mu s]$
P	power	$[W]$
U	electric potential difference	$[V]$
I	electric current	$[A]$
E	energy	$[J]$
V_r	volume of rock	$[m^3]$
SE	specific Energy	$[MPa]$

Appendix A

A.1 Correlation Tables – UCS Derived from Well Logs

Eq. No.	Region	Equation	Reference
1	Germany	$UCS = 0.035V_p - 31.5$	Freyburg (1972)
2	Australia	$UCS = 1200e^{-0.036\Delta t}$	McNally (1987)
3	Gulf Coast	$UCS = 1.4318 \times 10^7\, \Delta t^{-3}$	Unpublished
4	Gulf Coast	$UCS = 3.3 \times 10^{-20}\, \rho^2 {V_p}^4 \left[\frac{(1+\upsilon)}{(1-\upsilon)}\right]^2 (1-2\upsilon) \left[1 + 0.78V_{clay}\right]$	Fjaer et al. (1992)
5	Alaska	$UCS = 1.745 \times 10^{-9}\, \rho {V_p}^2 - 21$	Moos et al. (1999)
6	Australia	$UCS = 42.1e^{1.9\times10^{-11}\rho {V_p}^2}$	-
7	Gulf of Mexico	$UCS = 3.87e^{1.14\times10^{-10}\rho {V_p}^2}$	-
8	-	$UCS = 46.2e^{0.027E}$	Unpublished
9	Worldwide	$UCS = 2.28 + 4.1089E$	Bradford et al. (1998)
10	Sedimentary basins	$UCS = 254(1 - 2.7\phi)^2$	Vernik, Bruno et al. (1993)
11	-	$UCS = 277e^{-10\phi}$	-

Table 8. Empirical correlations between UCS and other measured physical parameters for sandstone

Units used: $V_p({}^{m}/_{s}), \Delta_t\left({}^{\mu s}/_{ft}\right), \rho\left({}^{kg}/_{m^3}\right), V_{clay}(fraction), E(MPa), \emptyset(fraction)$

Eq. No.	Region	Equation	Reference
12	North Sea	$UCS = 0.77(304.8/\Delta t)^{2.93}$	Horsrud (2001)
13	Gulf of Mexico	$UCS = 0.43(304.8/\Delta t)^{3.2}$	-
14	Globally	$UCS = 1.35(304.8/\Delta t)^{2.6}$	-
15	Gulf of Mexico	$UCS = 0.5(304.8/\Delta t)^{3}$	
16	North Sea	$UCS = 10(30438/\Delta t - 1)$	Lal (1999)
17	-	$UCS = 7.97e^{0.91}$	Horsrud (2001)
18	-	$UCS = 7.22e^{0.712}$	Horsrud (2001)
19	-	$UCS = 1.001\phi^{-1.143}$	Lashkaripour and Dusseault (1993)
20	North Sea	$UCS = 2.922\phi^{-0.96}$	Horsrud (2001)
21	-	$UCS = 0.286\phi^{-1.762}$	-

Table 9. Empirical correlations between UCS and other measured physical parameters for shale

Units used: $\Delta_t \left({}^{\mu s}/_{ft}\right), E(MPa), \emptyset(fraction)$

Eq. No.	Region	Equation	Reference
22	North Sea	$UCS = (7682/\Delta t)^{1.82}/145$	Militzer and Stoll (1973)
23	-	$UCS = 10^{(2.44+109.14/\Delta t)}/145$	Golubev and Rabinovich (1976)
24	-	$UCS = 13.8E^{0.51}$	-
25		$UCS = 25.1E^{0.34}$	-
26	Korobcheyev	$UCS = 276(1 - 3\phi)^2$	Rzhevsky and Novick (1971)
27	-	$UCS = 143.8e^{-6.95\phi}$	-
28	-	$UCS = 135.9e^{-4.8\phi}$	-

Table 10. Empirical correlations between UCS and other measured physical parameters for limestone and dolomite

Units used: $\Delta_t \left({}^{\mu s}/_{ft}\right), E(MPa), \emptyset(fraction)$

Appendix B

B.1 Cement Samples Prepared in the Laboratory

Figure 52. Soft cement

Figure 53. Hard Cement

Figure 54. 0B

Figure 55. 4B

Figure 56. 10B

B.2 Sample Material Provided by OMV

Figure 58. Pionier 47-19

Figure 57. Pionier 47-10

Figure 59. Pionier 47-16

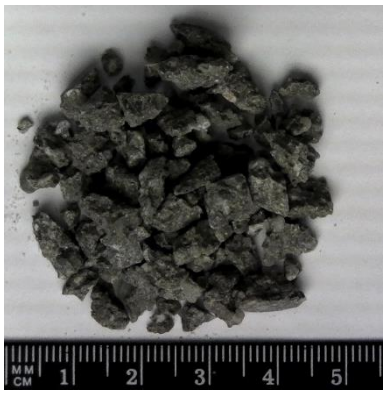

Figure 60. Ulrich 33

Figure 62. NH 35 Sandstone

Figure 61. Linenberg 03-1

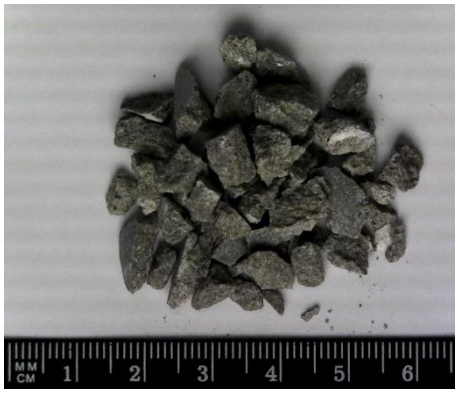

Figure 63. Ulrich 27

Figure 64. Linenberg 03-3

Figure 65. BS Sandstone

List of Figures

List of Tables